Available online at www.sciencedirect.com
SCIENCE DIRECT®
Inorganica Chimica Acta 358 (2005) 565–582
Inorganica Chimica Acta
www.elsevier.com/locate/ica

Copper(II) chloride/1-methylbenzotriazole chemistry: influence of various synthetic parameters on the product identity, structural and magnetic characterization, and quantum-chemical studies

Konstantina Skorda [a], Theocharis C. Stamatatos [a], Anastasios P. Vafiadis [b], Alexandra T. Lithoxoidou [b], Aris Terzis [c], Spyros P. Perlepes [a], Jerzy Mrozinski [d,*], Catherine P. Raptopoulou [c,*], John C. Plakatouras [e,*], Evangelos G. Bakalbassis [b,*]

[a] *Department of Chemistry, University of Patras, 265 04 Patras, Greece*
[b] *Laboratory of Applied Quantum Chemistry, Department of General and Inorganic Chemistry, Aristotle University of Thessaloniki, 541 24 Thessaloniki, Greece*
[c] *Institute of Materials Science, NCSR "Demokritos", 153 10 Aghia Paraskevi Attikis, Greece*
[d] *Institute of Chemistry, University of Wroclaw, 14 F. Joliot-Curie, 503 83 Wroclaw, Poland*
[e] *Department of Chemistry, University of Ioannina, 451 10 Ioannina, Greece*

Received 2 June 2004; accepted 22 September 2004
Available online 19 November 2004

Abstract

A systematic investigation of the $CuCl_2$/Mebta (Mebta = 1-methylbenzotriazole) reaction system is described, involving the determination of the influence of the Cu^{II}:Mebta ratio, the nature of solvent and the presence of counterions on the identity of the reaction products. As a consequence, complexes $[Cu_2Cl_4(Mebta)_4]$ (**1**), $[CuCl_2(Mebta)_2]$ (**2**), $\{[Cu_2Cl_4(Mebta)_2]\}_n$ (**3**), $[Cu_4OCl_6(Mebta)_4] \cdot 0.25H_2O$ (**4** · $0.25H_2O$) and $[Cu_2Cl_2(Mebta)_6](ClO_4)_2$ (**5**) have been isolated and structurally characterized by single-crystal X-ray studies. Mebta behaves as a monodentate ligand binding through N(3). **1** is a dinuclear complex, the structure of **2** consists of discrete monomeric units, and that of **3** is composed of linear, well-separated polymeric chains of Cu^{II} atoms. The molecules of **4** · $0.25H_2O$ have a central μ_4-oxide ion surrounded tetrahedrally by four Cu^{II} atoms. In the cations of **5** the two Cu^{II} centres are asymmetrically bridged by two chloro ligands, with three Mebta molecules completing five coordination at each metal. Complexes were characterized by spectroscopic (IR, far-IR, solution UV/Vis) and thermal decomposition (TG, DTG, and DTA) techniques. Variable-temperature magnetic susceptibility data for **1**, **3** and **5** showed intramolecular (**1**, **5**) and intrachain (**3**) ferromagnetic exchange interactions. Estimates of the *J* parameters, experimentally derived, were in close agreement with a new magneto-structural criterion developed by us, holding for bis(μ-chloro) copper(II) dimers. A comparison between the $CuCl_2$/Mebta and $CuBr_2$/Mebta systems is also presented.

Keywords: Bis(μ-chloro) copper(II) dimers; EHMO calculations; Ferromagnetic exchange interactions; (μ_4-oxo)hexakis(μ-chloro)tetracopper(II) core; 1-Methylbenzo triazole copper(II) complexes; One-dimensional copper(II) coordination polymers

1. Introduction

Our longstanding interest in the syntheses and properties of 3d-metal complexes with benzotriazole (btaH, Fig. 1) and its derivatives as organic ligands [1–5] has been stimulated by a variety of factors, not least of

* Corresponding authors. Tel.: +30 231 099 7695; fax: +30 231 099 7738(Evangelos G. Bakalbassis).
E-mail addresses: jmroz@wchuwr.chem.uni.wroc.pl (J. Mrozinski), craptop@demokritos.gr (C.P. Raptopoulou), iplakatu@cc.uoi.gr (J.C. Plakatouras), bakalbas@chem.auth.gr (E.G. Bakalbassis).

0020-1693/$ - see front matter © 2004 Elsevier B.V. All rights reserved.
doi:10.1016/j.ica.2004.09.042

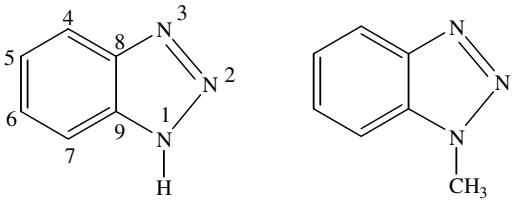

Fig. 1. Benzotriazole (btaH) and 1-methylbenzotriazole (Mebta).

which is the relevance of this area to the protection of metal surfaces against wear and corrosion. The anti-corrosion properties of btaH and its benzene ring-substituted derivatives toward certain metals, particularly copper and its alloys, are well established [6–8]. It has been postulated that copper oxide films are prerequisites for corrosion inhibition [9] and practical use of btaH as a corrosion inhibitor involves application to copper surfaces which have undergone some degree of oxidation. Despite the importance of benzotriazole corrosion inhibitors, no final conclusions have been reached of how they bind to oxidized metal surfaces, and why seemingly minor modifications in the structures of corrosion inhibitors can have a profound effect on their efficacy. Inorganic chemistry groups [10,11], including our group [1,4], have been investigating the mode of interaction of benzotriazoles with lightly oxidized metal surfaces by studying the coordination chemistry of these ligands with complexes of metal ions bound to oxygen-donor ligands. Garner's and Tasker's groups illustrated a new approach, based on the synthesis of polynuclear copper(II) benzotriazolato complexes containing β-diketonates as coligands, and the use of structural motifs found in such complexes to model relevant surface interactions, and hence understand the mode of action of benzotriazole inhibitors [10].

Another reason for the intense current interest in the coordination chemistry of benzotriazoles is the fact that benzotriazolate ligands are among the important players in the field of polynuclear transition metal chemistry. The development of routes and strategies for the synthesis of polynuclear complexes (clusters) of 3d metals (especially in moderate oxidation states) has been a subject of increasing interest over the last 15 years. These compounds provide a substantial impetus to several scientific areas, including bioinorganic chemistry, solid-state physics, molecular magnetism and material science [12–14]. For example, we have shown that the systematic investigation of the [Ni(β-diketonate)$_2$L$_2$]-RbtaH or btaOH reaction mixtures has led to four families of polynuclear complexes: [Ni$_5$(OH)(acac)$_4$(Rbta)$_5$S$_4$] [4], [Ni$_5$(dbm)$_4$(Rbta)$_6$S$_4$] [15], [Ni$_7$(OH)$_2$(acac)$_8$(btaO)$_4$S$_2$] [1] and [Ni$_9$(bzac)$_6$(Rbta)$_{12}$S$_6$] [15] (acacH = acetylacetone; btaOH = 1-hydroxybenzotriazole; bzacH = benzoylacetone; dbmH = dibenzoylmethane; L = H_2O, EtOH; RbtaH = 5-methyl-, 6-methyl-, 5,6-dimethyl-, 5-chlorobenzotriazole or benzotriazole; S = solvate ligands). These complexes have novel structures and interesting magnetic properties. Recently, excellent synthetic work in Mn chemistry from Brechin's group has resulted in the isolation of benzotriazolate-bridged Mn_{26}^{III} [16], $Mn_{10}^{III}Mn_3^{IV}$ [17] and Mn_8^{III} [17] clusters with impressive structures and exciting magnetic properties, including [16] single-molecule magnet [13] behaviour.

1-Methylbenzotriazole (Mebta, Fig. 1) is not an efficient corrosion inhibitor. No coordination mode of Mebta other than monodentate binding through N(3) was found to occur in iron(III), cobalt(II), nickel(II), copper(II), palladium(II) and platinum(II) chemistries [3,5]. Thus, monodentate N(3) coordination can be regarded as the only coordination mode of Mebta and N(1)-substituted benzotriazoles (with groups containing no donor atoms). This monodentate coordination accounts in part for the lack of long-term corrosion inhibition on metals by Mebta [8]. For $CuBr_2$ and Mebta, our studies showed [3] that the Mebta:Cu^{II} ratio and the nature of solvent affect the identity of the reaction products. Combined variations of these synthetic parameters led to the isolation of the complexes $\{[CuBr_2(Mebta)]\}_n$, $[CuBr_2(Mebta)_2]$, $[CuBr_2(Mebta)(MeCN)]$ and $[CuBr_2(Mebta)_3]$. We decided to study the $CuCl_2$/Mebta reaction system to investigate the effect of halide substitution upon both the structural and physical properties of the resulting complexes. As far as the physical properties are concerned, differences might be expected. For instance, Hatfield, Hodgson and their coworkers, in their studies [18] on five-coordinate dinuclear bis(μ-chloro)copper(II) complexes of the types $[CuCl_2L_2]_2$ and $[CuCl_2(L–L)]_2$ (L and L–L are monodentate and bidentate chelating ligands, respectively), found a strong correlation between the exchange coupling constant, $2J$, and the structural parameter φ/R (where φ is the Cu–Cl–Cu bridging angle and R is the longest bond in the $Cu_2(\mu\text{-}Cl)_2$ unit). However, in the case of the bromo analogues, Landee and Greeney [19] showed that the dominant factor controlling superexchange strength is not related to the bridging angle but instead to the amount of distortion within the copper(II) basal plane; a later study by Romero et al. [20], however, showed that magnetic interaction strength can be correlated to the arrangement of the bridging bromo ligands around the metal.

In this report, we present our results from the full investigation of the $CuCl_2$/Mebta reaction system. As we shall describe, we have found a number of synthetic parameters to have a great effect on the structure of obtained products. Detailed variable-temperature magnetic susceptibility and EPR studies will also be presented for three representative complexes, as well as a quantum-chemical interpretation of the exchange cou-

pling. Some preliminary results of this work have already been briefly communicated [21].

2. Experimental

2.1. Reagents and physical measurements

All manipulations were performed under aerobic conditions. Starting materials and solvents were commercially available and used without further purification. Mebta was purchased from Lancaster Synthesis Ltd.

Microanalyses (C, H, N) were performed by the University of Ioannina Microanalytical Laboratory using an EA 1108 Carlo Erba analyser. Thermogravimetric (TG), differential thermogravimetric (DTG) and differential thermal analysis (DTA) data were obtained on Dupont R90 (equipped with a 951 TG analyser) and Seiko 200 TG/DTA instruments in a dinitrogen gas flow (50 cm^3 min^{-1}); sample weights of 5–10 mg and heating rates of 1 and 5 °C min^{-1} were used. IR spectra (4000–500 cm^{-1}) were recorded on a Perkin–Elmer 16 PC FT spectrometer with samples prepared as KBr pellets. FT far-IR spectra were recorded on a Bruker IFS 113v spectrometer with samples prepared as polyethylene pellets. Solution electronic spectra (800–300 nm) were recorded on a Biochrom 4060 instrument. Variable-temperature (293–4.2 K) magnetic susceptibility measurements were carried out on polycrystalline samples by the Faraday method using a sensitive Sartorius M-25D electrobalance; the instrument was standardized with $HgCo(NCS)_4$. The applied magnetic field was 6.25 KOe. The experimental molar magnetic susceptibilities were corrected for the diamagnetic response using Pascal's constants. The value of 60×10^{-6} cm^3 mol^{-1} was used for the TIP of the copper(II) ion. The magnetism of the samples was found to be field-independent. Variable-temperature (300–77 K) EPR spectra were recorded on a Bruker ER 200E-SRC X-band spectrometer; DPPH was used as an external standard. EPR spectra at the liquid He temperature were recorded on a Radiopan SE/X 2543 X-band spectrometer; DPPH was used as reference, and the magnetic field was calibrated with proton and lithium NMR probes.

Safety note. Benzotriazoles and their metal complexes are potentially explosive, and caution should be exercised in handling such compounds. However, the small quantities used in this study were not found to present a hazard.

2.2. Computational details

Calculations were carried out with the parametrization and methods already described [22]. In particular, EHMO SCC calculations [23–25] were performed on the $[Cu_2Cl_4(NH_3)_4]$ model dimer in an attempt to determine the H_{ii}s of the atoms, by using the FORTICON MAC program [26]. The off-diagonal matrix elements were given by the expression of Wolfsberg–Helmholz [27]; still a value of 1.75 for the parameter K was used. The orbital exponents for the atoms were 1.625 for C, 1.95 for N, 2.033 for Cl, 1.30 for H, 2.05 and 1.325 for the 4s and 4p ones of Cu, respectively, as well as two-component 3d orbital of Cu with exponents of 5.95 and 2.30 and relative weights of 0.5933 and 0.5744, respectively.

2.3. Compound preparation

2.3.1. *[Cu_2Cl_4(Mebta)$_4$] (**1**)*

To a colourless solution of Mebta (0.25 g, 1.88 mmol) in EtOH (45 ml) was added a green solution of $CuCl_2 \cdot 2H_2O$ (0.16 g, 0.94 mmol) in the same solvent (45 ml). The green solution obtained was stirred at ambient temperature for 1–2 min and allowed to stand undisturbed for 24 h. Bluish green crystals of the product slowly appeared, which were collected by filtration, washed with EtOH (5 ml) and Et_2O (2 × 10 ml), and dried in air. Yield: 62%. *Anal.* Calc. for $C_{28}H_{28}N_{12}Cl_4Cu_2$: C, 42.0; H, 3.5; N, 21.0. Found: C, 41.8; H, 3.6; N, 20.4%. Crystals suitable for single-crystal X-ray crystallography were isolated by layering a solution of the product in MeOH with a mixture of Et_2O and *n*-hexane. Selected IR spectral data (KBr, cm^{-1}): 3053 w, 3037 m, 1497 m, 1480 s, 1392 m, 1230 s, 1140 m, 1052 s, 759 vs, 748 sh, 664 w. Selected far-IR spectral data (polyethylene, cm^{-1}): 299 sb, 271 sh, 265 m, 180 m, 162 s. UV/Vis spectral data (MeOH, kK): 26.52, 12.31. Complex **1** can also be prepared by employing Mebta:$CuCl_2 \cdot 2H_2O$ ratios of 8:1 and 4:1 in EtOH or MeOH.

2.3.2. *[$CuCl_2$(Mebta)$_2$] (**2**)*

A slurry of $CuCl_2 \cdot 2H_2O$ (0.16 g, 0.94 mmol) in MeCN (50 ml) was refluxed for 5–6 h to give a clear yellow solution. This solution was added to a solution of Mebta (0.25 g, 1.88 mmol) in MeCN (20 ml) under stirring. The resulting green solution was left undisturbed at ambient temperature for 24 h and during this time bluish green crystals of **1** appeared. This material was completely transformed into X-ray quality green crystals of the product over a period of 3 days. The crystals were collected by filtration, washed with MeCN (2 × 10 ml) and Et_2O (210 ml), and dried in vacuo over silica gel. Yield: 63%. *Anal.* Calc. for $C_{14}H_{14}N_6Cl_2Cu$: C, 42.0; H, 3.5; N, 21.0. Found: C, 41.7; H, 3.3; N, 20.5%. Selected IR spectral data (KBr, cm^{-1}): 3057 w, 2932 w, 1494 w, 1458 m, 1385 s, 1222 s, 1132 m, 1050 s, 779 m, 750 s, 657 w. UV/Vis spectral data (MeOH, kK): 24.31, 11.50. Effective magnetic moment per copper(II): 2.12 BM at 22 °C. Complex **2** can also be isolated by employing Mebta:$CuCl_2 \cdot 2H_2O$ ratios of 8:1, 6:1, 4:1 and 1:1 in MeCN. The 8:1, 6:1, 4:1, 2:1 and 1:1 reactions

in $MeNO_2$ also give complex **2** in completely similar procedures to those in MeCN (through the intermediate appearance of the bluish green crystals of **1**). Employment of MeOH or EtOH as solvents can also lead to **2**. The 8:1, 6:1, 4:1 and 2:1 reactions between Mebta and $CuCl_2 \cdot 2H_2O$ in MeOH or EtOH give initially complex **1** under the conditions described above. When the reaction mixture is allowed to slowly concentrate at room temperature, green crystals of **2** also form. The not-too-dissimilar solubility of **1** and **2** prevents chemical separation. The two products are readily separated manually, washed with a little alcohol and Et_2O, dried in air and can individually be identified as complexes **1** and **2** by unit cell determination and spectral comparison with authentic materials.

2.3.3. $\{[Cu_2Cl_4(Mebta)_2]\}_n$ (3)

Method A. This compound was initially prepared as a powder by the thermal decomposition of the dinuclear complex $[Cu_2Cl_4(Mebta)_4]$ (**1**). The TG/DTG/DTA curves of the latter showed a first endothermic weight loss between 150 and 203 °C, which corresponds to the elimination of two moles of Mebta per mole of **1** (Calc.: 33.2; Found: 32.1%). This first decomposition possibly consists of two overlapping steps as indicated by the appearance of a shoulder in the main DTG peak. A small but well-defined TG plateau is reached at 205 up to 215 °C. The thermally stable brown intermediate, obtained after an isothermal TG experiment at 205 °C, was isolated and studied by IR, far-IR and UV/Vis spectroscopic methods; this study proved the intermediate to be compound **3** (see Method B).

Method B. A solution of Mebta (0.25 g, 1.88 mmol) in EtOH (35 ml) was added to a green solution of $CuCl_2 \cdot 2H_2O$ (0.64 g, 3.75 mmol) in the same solvent (35 ml) under stirring. A deep green homogeneous solution was obtained, which after few hours began to deposit a brown powder. The flask was stored at ambient temperature overnight, and the precipitate was collected by filtration, washed with EtOH (10 ml) and Et_2O (2×10 ml), and dried in vacuo over silica gel. Yields as high as 70% were obtained. *Anal.* Calc. for $C_{14}H_{14}N_6Cl_4Cu_2$: C, 31.4; H, 2.6; N, 15.7. Found: C, 31.3; H, 2.5; N, 15.3%. Crystals suitable for X-ray crystallography were obtained by mixing a solution of Mebta (0.20 g, 1.50 mmol) in EtOH (30 ml) with a solution of $CuCl_2 \cdot 2H_2O$ (0.26 g, 1.53 mmol) in the same solvent (60 ml). The flask was stored at ambient temperature for 10 h. An approximately 5:1 mixture of brown and bluish green crystals formed. The two products were readily separated manually, washed with a little EtOH and Et_2O (not added in the filtrate), dried in air and individually identified as complexes **3** (by single-crystal X-ray crystallography) and **1** (by spectral comparison with authentic material), respectively. Overnight storage of the filtrate at 20 °C yielded a second crop of crystals of **3** only, i.e., not contaminated with **1**. Selected IR spectral data (KBr, cm^{-1}): 3058 w, 2942 w, 1497 m, 1460 s, 1392 w, 1225 s, 1141 m, 1052 m, 785 m, 748 s, 664 w. Selected far-IR spectral data (polyethylene, cm^{-1}): 287 s, 175 sh, 159 s. UV/Vis spectral data (DMF, kK): 30.95, 22.95, 12.50.

2.3.4. $[Cu_4OCl_6(Mebta)_4] \cdot 0.25H_2O$ ($4 \cdot 0.25H_2O$)

Method A (in a mixture with complexes 1 and 3). A green solution of $CuCl_2 \cdot 2H_2O$ (0.25 g, 1.47 mmol) in EtOH (40 ml) was added to a stirred solution of Mebta (0.20 g, 1.50 mmol) in the same solvent (20 ml). The resulting green solution was stirred for 5 min, and left capped and undisturbed for 2 weeks. This prolonged storage gave a mixture of bluish green prisms, brown prisms and brown needles. These different forms were carefully collected by filtration and dried in air. The three products were separated manually and individually identified as complexes **1** (by spectral comparison with authentic material), **3** (by unit cell determination) and $\mathbf{4} \cdot 0.25H_2O$ (by single-crystal X-ray crystallography), respectively. Typical yields were ~10% (**1**), 30% (**3**) and 20% ($\mathbf{4} \cdot 0.25H_2O$).

Method B. CuO (0.09 g, 1.19 mmol) was added to a brown solution of $CuCl_2$ (0.32 g, 2.38 mmol) in MeOH (20 ml). The resulting brown slurry was refluxed for 24 h to give a cloudy brown "solution". This was filtered and a solution of Mebta (0.40 g, 3.00 mmol) in MeOH (5 ml) added to the filtrate. No noticeable colour change occurred. The new solution obtained soon began to deposit a fine brown powder. The slurry was stirred until the reaction appeared complete and then filtered. The brown precipitate of the product was washed with cold MeOH (5 ml) and Et_2O (2×5 ml), and dried in air. Yield: 43%. *Anal.* Calc. for $C_{28}H_{28.5}N_{12}O_{1.25}Cl_6Cu_4$: C, 33.0; H, 2.8; N, 16.5. Found: C, 33.2; H, 2.9; N, 17.0%. Selected IR spectral data (KBr, cm^{-1}): 3057 w, 2932 w, 1497 m, 1460 m, 1397 m, 1230 s, 1141 w, 1125 w, 1057 m, 779 sh, 748 s, 664 w. Selected far-IR spectral data (polyethylene, cm^{-1}): 575 s, 274 m, 231 s, 191 w. UV/Vis spectral data (MeCN, kK): 27.40 sh, 12.50. Effective magnetic moment per copper(II): 1.90 BM at 20 °C.

2.3.5. $[Cu_2Cl_2(Mebta)_6](ClO_4)_2$ (5)

To a stirred solution of Mebta (0.24 g, 1.80 mmol) in commercial concentrated hydrochloric acid (3 ml) was added a sky blue solution of $CuCl_2 \cdot 2H_2O$ (0.12 g, 0.70 mmol) in H_2O (7 ml). The colour of the solution immediately changed to green. This was stirred, while an aqueous solution (2 ml) of $NaClO_4 \cdot H_2O$ (0.15 g, 1.07 mmol) was added to give a new solution of the same colour. The reaction flask was allowed to stand undisturbed at ambient temperature for 10–12 h. During this time X-ray quality green crystals of the product formed. The crystals were collected by fil-

tration, washed with EtOH (3×10 ml) and dried in vacuo over silica gel. Yield: 57%. *Anal.* Calc. for $C_{42}H_{42}N_{18}O_8Cl_4Cu_2$: C, 42.2; H, 3.5; N, 21.1. Found: C, 42.1; H, 3.4; N, 20.7%. Selected IR spectral data (KBr, cm^{-1}): 3052 w, 2935 w, 1502 m, 1460 s, 1397 m, 1230 s, 1146 s, ~1100 sb, 785 m, 748 s, 664 w, 630 s. Selected far-IR spectral data (polyethylene, cm^{-1}): 275 sb, 188 m, 167 s. UV/Vis spectral data (DMF, kK): 27.02, 23.00, 12.20.

2.4. X-ray crystallography

Data collection, crystal data and structure solution information are listed in Table 1. Diffraction measurements for compounds **1**, **3**, **4** · $0.25H_2O$, and **5** were performed on a $P2_1$ Nicolet diffractometer using Zr-filtered Mo Kα radiation, while for compound **2** the data collection was performed on a Crystal Logic Dual Goniometer diffractometer using graphite monochromated Mo Kα radiation. Unit cell dimensions were determined and refined by using the angular settings of 25 automatically centred reflections. Intensity data were recorded using a θ–2θ scan. Three standard reflections monitoring every 97 reflections showed less than 3% variation and no decay. Lorentz, polarization and Ψ-scan absorption corrections (for **1**–**4** only) were applied.

The structures were solved by direct methods using SHELXS-86 [28] and refined by full-matrix least-squares techniques of F^2 with SHELXL-97 [29]. For **1**, **2**, **3** and **5** all H atoms were located by difference maps and refined isotropically; all non-H atoms were refined with anisotropic thermal parameters. For **4** · $0.25H_2O$ all H atoms were located by difference maps and refined isotropically, except those on the methyl groups which were introduced at calculated positions as riding on bonded atoms; all non-H atoms were refined anisotropically, except the oxygen of the solvate H_2O molecule which was refined isotropically.

3. Results and discussion

3.1. Syntheses

The product identity of the $CuCl_2 \cdot 2H_2O$/Mebta reaction systems depends mainly on the metal:ligand reaction ratio and the nature of the solvents. The various synthetic procedures and transformations described in detail in Section 2.3 are conveniently summarized in the stoichiometric chemical Eqs. (1)–(8). It should be pointed out that Eqs. (2) and (4) represent chemical equilibria in solution, while Eq. (3) [which, at first

Table 1
Crystallographic data for complexes **1**, **2**, **3**, **4** · $0.25H_2O$ and **5**

	1	**2**	**3**	**4** · $0.25H_2O$	**5**
Empirical formula	$C_{28}H_{28}Cu_2N_{12}Cl_4$	$C_{14}H_{14}CuN_6Cl_2$	$C_{14}H_{14}Cu_2N_6Cl_4$	$C_{28}H_{28.5}Cu_4N_{12}O_{1.25}Cl_6$	$C_{42}H_{42}Cu_2N_{18}O_8Cl_4$
Formula weight	801.50	400.75	535.20	1019.99	1195.82
Crystal system	monoclinic	triclinic	monoclinic	orthorhombic	triclinic
Space group	$P2_1/n$	$P\bar{1}$	$I/2m$	$Pccn$	$P\bar{1}$
a (Å)	9.927(1)	10.668(7)	8.877(1)	11.688(1)	8.197(2)
b (Å)	15.627(1)	8.617(6)	7.113(1)	17.078(1)	11.740(2)
c (Å)	10.753(1)	9.157(6)	14.876(1)	19.368(1)	13.787(2)
α (°)		82.12(2)			70.89(1)
β (°)	96.69(1)	87.44(2)	93.94(1)		89.54(1)
γ (°)		83.38(2)			101.22(1)
U ($Å^3$)	1656.7(2)	827.9(10)	937.0(2)	3866.1(4)	1226.0(4)
Z	2	2	2	4	1
D_{calc} (g cm^{-3})	1.607	1.608	1.897	1.752	1.620
T (K)	298	298	298	298	298
λ^aÅ)	0.71073	0.71073	0.71073	0.71070	0.71070
μ (mm^{-1})	1.647	1.648	2.851	2.628	1.158
θ range (°)	2.95–27.00	1.92–26.00	3.18–27.00	2.36–24.99	1.57–25.00
Octants collected	±h, k, l	−h, ±k,±1	±h, k, l	h, k, l	±h, ±k, l
Collected reflections	4042	3434	1134	1982	4810
Unique reflections (R_{int})	3600 (0.0181)	3428 (0.0155)	1093 (0.0141)	1982 (0.0000)	4327 (0.0206)
Number of refined parameters	264	264	97	270	418
Observed reflections[b]	3068	2948	1015	1982	3646
R^{1c}, wR^{2d} [$I > 2\sigma(I)$]	0.0239, 0.0681	0.0299, 0.0787	0.0219, 0.0646	0.0381, 0.0790	0.0319, 0.0809
GoF (on F^2)	1.065	1.082	1.117	1.099	1.067
($\Delta\rho_{max}$) ($\Delta\rho_{min}$) (e $Å^{-3}$)	0.299, −0.287	0.268, −0.479	0.363, −0.383	0.447, −0.309	0.408, −0.247

[a] Mo Kα radiation.
[b] $I > 2\sigma(I)$.
[c] $R_1 = \sum(|F_o| - |F_c|)/\sum(|F_o|)$.
[d] $wR_2 = \{\sum[w(F_o^2 - F_c^2)^2]/\sum[w(F_o^2)^2]\}^{1/2}$.

glance, is similar to Eq. (4)] represents the solid-state reaction described in Method A of Section 2.3.3. Concerning Eq. (8), we believe that HCl is not taking part in the reaction mechanism and it just assists the dissolution of Mebta

$$2CuCl_2 \cdot 2H_2O + 4Mebta \xrightarrow{ROH} [Cu_2Cl_4(Mebta)_4] + 4H_2O \quad (1)$$

$$[Cu_2Cl_4(Mebta)_4] \overset{ROH}{\rightleftharpoons} 2[CuCl_2(Mebta)_2] \quad (2)$$

$$n[Cu_2Cl_4(Mebta)_4] \xrightarrow[N_2]{150-205^\circ C} \{[Cu_2Cl_4(Mebta)_2]\}_n + 2n\,Mebta \uparrow \quad (3)$$

$$n[Cu_2Cl_4(Mebta)_4] \overset{EtOH}{\rightleftharpoons} \{[Cu_2Cl_4(Mebta)_2]\}_n + 2n\,Mebta \quad (4)$$

$$2nCuCl_2 \cdot 2H_2O + 2n\,Mebta \xrightarrow[exc.\ CuCl_2\cdot 2H_2O]{EtOH} \{[Cu_2Cl_4(Mebta)_2]\}_n + 4nH_2O \quad (5)$$

$$4CuCl_2 \cdot 2H_2O + 4Mebta \xrightarrow{EtOH} [Cu_4OCl_6(Mebta)_4] \cdot 0.25H_2O + 2HCl + 6.75H_2O \quad (6)$$

$$3CuCl_2 + CuO + 4Mebta + 0.25H_2O \xrightarrow[T]{MeOH} [Cu_4OCl_6(Mebta)_4] \cdot 0.25H_2O4 \cdot 0.25H_2O \quad (7)$$

$$2CuCl_2 \cdot 2H_2O + 6Mebta + 2NaClO_4 \cdot H_2O \xrightarrow{HCl\ 3N} [Cu_2Cl_2(Mebta)_6](ClO_4)_2 + 2NaCl + 6H_2O \quad (8)$$

3.2. Description of structures

Selected interatomic distances and angles for complexes **1**, **2**, **3**, **4** · 0.25H_2O and **5** are listed in Tables 2–4, 6 and 8, respectively. Labelled ORTEP plots of these complexes are shown in Figs. 2–6. There are two common features in the five structures. Firstly, Mebta behaves as a monodentate ligand with the nitrogen atom of position 3 (Fig. 1) being the ligated atom; secondly, the molecules of Mebta are essentially planar, the deviations of atoms from the least-squares plane through them being less than 0.02 Å.

The crystal structure of **1** consists of isolated dinuclear molecules with two bridging chloro ligands; a terminal chloride and two nitrogen atoms from two *trans*-Mebta ligands complete five-coordination at each metal ion. The bridging CuCl(1)Cu′Cl(1′) unit is strictly planar, with a crystallographically imposed inversion

Table 2
Selected interatomic distances (Å) and angles (°) for complex **1**

Cu–Cl(1)	2.302(1)	Cu–N(3)	2.021(1)
Cu–Cl(1′)	2.629(1)	Cu–N(13)	2.023(1)
Cu–Cl(2)	2.273(1)	Cu…Cu′	3.437(1)
Cl(1′)–Cu–Cl(1)	91.9(1)	Cl(1)–Cu–N(13)	89.1(1)
Cl(1′)–Cu–Cl(2)	100.5(1)	Cl(2)–Cu–N(3)	90.1(1)
Cl(1′)–Cu–N(3)	94.3(1)	Cl(2)–Cu–N(13)	90.1(1)
Cl(1′)–Cu–N(13)	93.2(1)	N(3)–Cu–N(13)	172.3(1)
Cl(1)–Cu–Cl(2)	167.6(1)	Cu–Cl(1)–Cu′	88.1(1)
Cl(1)–Cu–N(3)	89.0(1)		

Symmetry code: ′ = $-x$, $-y$, $-z$ + 1.

Table 3
Selected bond distances (Å) and angles (°) for complex **2**

Cu–Cl(1)	2.228(2)	Cu–N(3)	1.981(2)
Cu–Cl(2)	2.230(1)	Cu–N(13)	1.990(2)
Cl(1)–Cu–Cl(2)	143.7(1)	Cl(2)–Cu–N(3)	94.8(1)
Cl(1)–Cu–N(3)	93.8(1)	Cl(2)–Cu–N(13)	93.6(1)
Cl(1)–Cu–N(13)	95.0(1)	N(3)–Cu–N(13)	152.3(1)

Table 4
Selected interatomic distances (Å) and angles (°) for complex **3**

Cu(1)–Cl	2.261(1)	Cu(2)–N(3)	1.986(2)
Cu(2)–Cl	2.534(1)	Cu(1)…Cu(2)	3.556(1)
Cl–Cu(1)–Cl	90.3(1)	Cl–Cu(2)–N(3)	89.4(1)
Cl–Cu(2)–Cl	78.5(1)	Cu(1)–Cl–Cu(2)	95.6(1)

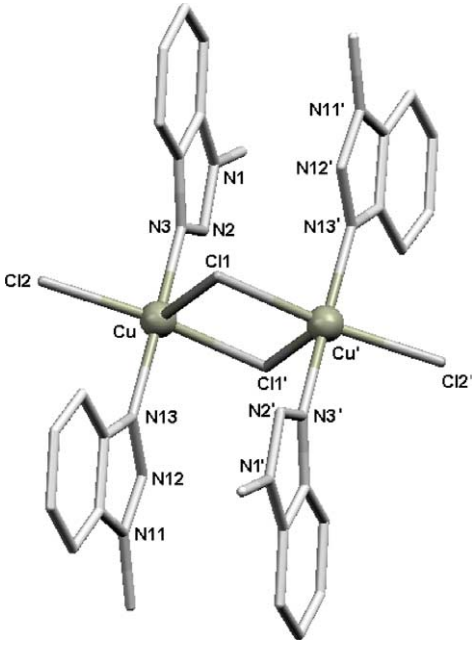

Fig. 2. Partially labelled ORTEP representation of the dinuclear molecule of complex **1** at the 30% probability level. Primed and unprimed atoms are related by the crystallographic inversion centre.

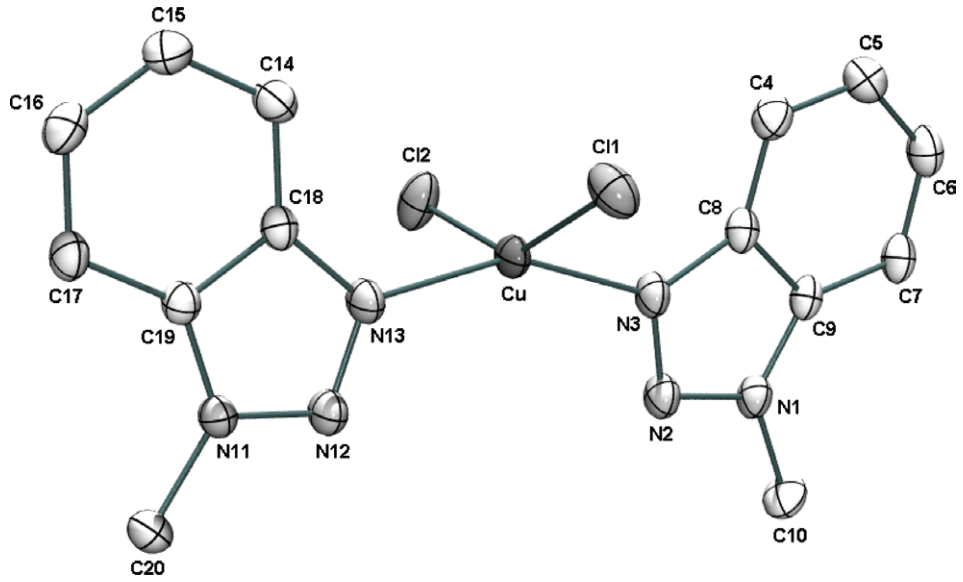

Fig. 3. Molecular structure of **2** with the atom labelling scheme. The atoms are drawn at the 30% probability level.

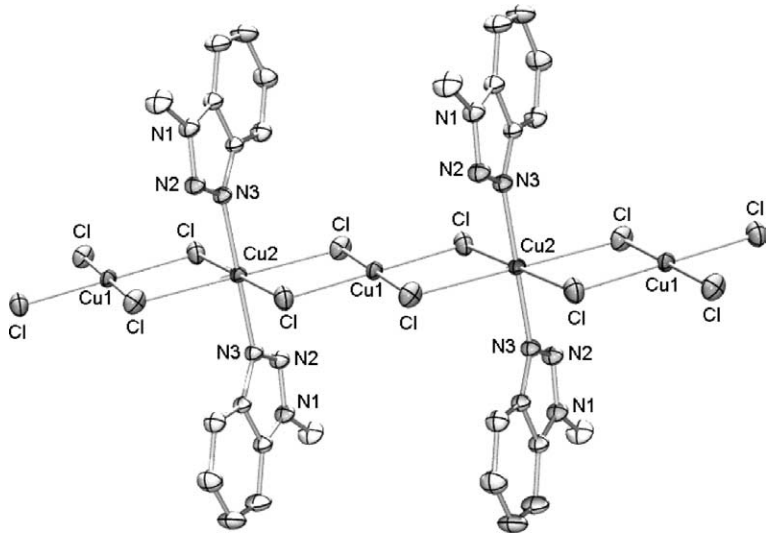

Fig. 4. A small portion of the chain present in complex **3**. Carbon atoms are not labelled; identical labels are used for symmetry-generated atoms. The atoms are drawn at the 30% probability level.

centre in the middle of the dimer. The geometry at each Cu^{II} centre is square pyramidal (sp) with the basal plane comprising the two *trans*-nitrogen atoms and two *trans*-chloride ions [Cl(1) and Cl(2) for Cu]; the apical position is occupied by the chloro ligand [Cl(1′) for Cu] which is basal to the other copper (Cu′) in the dimer.

The in-plane Cu–Cl distances of 2.273(1) and 2.302(1) Å are within the normal range, with the distance to the bridging chlorine slightly longer, as expected. The Cu…Cu′ separation [3.437(1) Å], the out-of-plane Cu–Cl(1′) distance [2.629(1) Å] and the bridging Cu–Cl(1)–Cu′ angle [88.1°] in **1** are all towards the low end of the respective ranges observed for other, structurally similar square-pyramidal dichloro-bridged copper(II) dimers [18,30–33].

The Mebta ligands in *syn* positions are nearly parallel, the angle between their mean planes being 4.3°. There appear to be intradimer stacking interactions between these ligands on the two sides of the molecule; the shortest distance from the mean plane of N(1), N(2), and N(3) – containing Mebta ligands is 3.50 Å for N(12′).

Complex **1** joins a rather large family of structurally characterized complexes of the type $[Cu_2Cl_2(\mu\text{-}Cl)_2L_x]$ ($x = 2$, 4) [18,30–33]. However, most members of this family contain bidentate chelating ligands Ls ($x = 2$); complexes containing monodentate aromatic N-donors

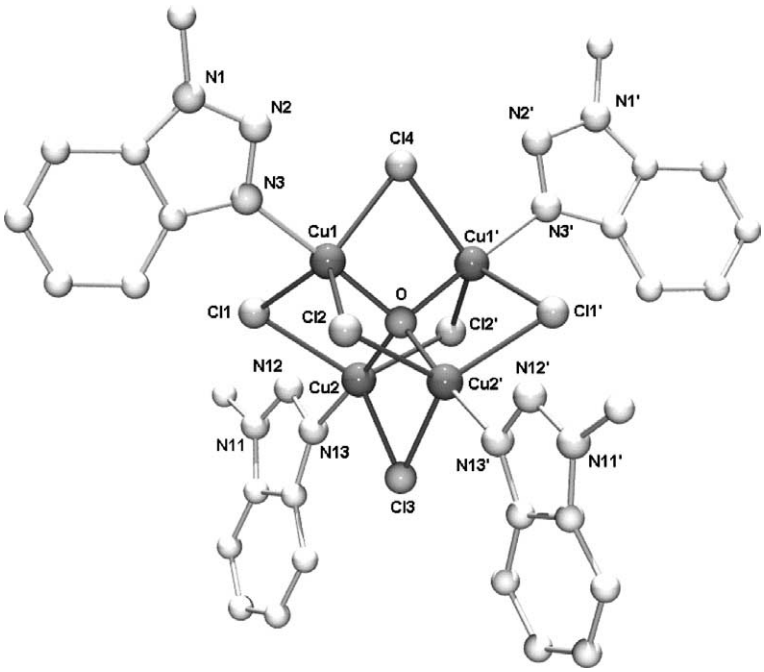

Fig. 5. Molecular structure of complex **4**. Primes are used for symmetry-related atoms. The carbon atoms are not labelled for clarity.

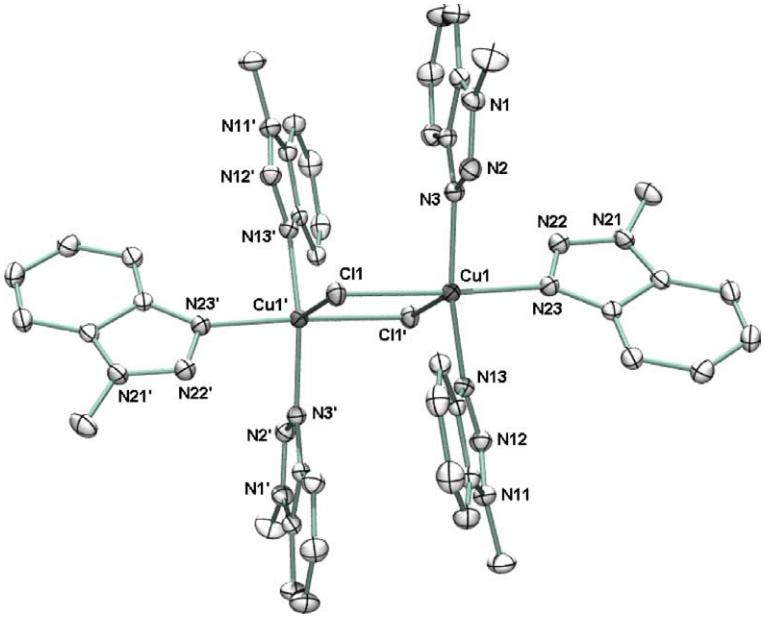

Fig. 6. Partially labelled ORTEP plot for the dinuclear cation of complex **5** at the 30% probability level. Primed and unprimed atoms are related by the crystallographic inversion centre.

($x = 4$) are rare, a typical example being $[Cu_2Cl_4(2\text{-pic})_4]$ (2-pic = 2-methylpyridine) [32]. In this complex, the apical Cu–Cl bond [3.364(1) Å] is extremely long and longer than that found in any other square-pyramidal dichloro-bridged copper(II) dimer.

The Cu^{II} atom in the mononuclear complex **2** is surrounded by two nitrogen atoms and two terminal chloro ligands. The geometry about the copper ion is best described as tetrahedrally distorted *trans*-square planar. The *cis* [93.6(1)–95.0(1)°] and *trans*-angles [143.7(1) and 152.3(1)°] of all ligands around the metal ion are intermediate between the expected values for tetrahedral (109.47°) and square planar (90°, 180°), respectively. The two Cu–Cl distances [2.228(2) and 2.230(1) Å] are typical for terminal Cu–Cl bonds [34]. The Cu–N distances [1.981(2) and 1.990(2) Å] are very close to the

Cu–N bond lengths of 1.968(4) and 1.970(4) Å in the isostructural complex $[CuBr_2(Mebta)_2]$ [3].

A very close precedent to **2** is complex $[CuCl_2(mim)_2]$ (mim = *N*-methylimidazole), in which the average Cu–Cl and Cu–N bond lengths, and the Cl–Cu–Cl and N–Cu–N angles are 2.258(3), 1.969(5) Å, 143.6(1) and 149.7(1)°, respectively [34].

The crystal structure of complex **3** is composed of well-separated, linear chains of Cu^{II} atoms bridged asymmetrically by two chloro ligands. A regular alternation of two non-equivalent copper(II) ions [Cu(1) and Cu(2)] occurs in the chain; Cu(1) is surrounded by four chlorides in an almost perfect square-planar environment, whereas Cu(2) exhibits a compressed, *trans*-octahedral $(\mu\text{-Cl})_4N_2$ environment. There is a mirror plane through Cu(2) and the Mebta ligands, and a second one, parallel to the first, through Cu(1), as well as a twofold crystallographic axis perpendicular to the mirror planes through Cu(1) and Cu(2). Thus, each Cu^{II} atom is located on a crystallographic centre of symmetry; the two local inversion centres result in only one crystallographically independent chloride atom and Mebta ligand. The Cu(1)–Cl bond distance [2.261(1) Å] is noticeably shorter than the Cu(2)–Cl bond length [2.534(1) Å], consistent with the lower coordination number for Cu(1).

The doubly bridged chain with two alternating chromophores observed in **3** is unique for complexes of the formulation CuX_2L (X = Cl or Br, L = monodentate ligand). Most of the bis(μ-Cl) 1D copper(II) complexes have the formulations $CuCl_2L_2$ or $CuCl_2$(L–L), where L–L is a bidentate chelating ligand, and contain exclusively six-coordinate metal ions. In Table 5 are compared selected structural parameters for **3** and representative bis(μ-chloro) copper(II) chains of the general formula $\{[CuCl_2L_2]\}_n$.Complex **3** exhibits the shortest Cu–Cl and Cu...Cu distances and the largest Cu–Cl–Cu angle.

It should be pointed out at this point that powders of empirical formulae $CuCl_2(Mebta)_2$ and $CuCl_2(Mebta)$ have been known since 1983 when Reedijk et al. [11] isolated them from the reactions of $CuCl_2 \cdot 2H_2O$ and Mebta in EtOH/*n*-pentane. The authors proposed a chloro-bridged linear-chain structure with two monodentate Mebta ligands per Cu^{II} for the 1:2 complex, and suggested a bidentate bridging mode of Mebta in the 1:1 compound; with hindsight, it seems that the 1:1 compound is complex $\{[Cu_2Cl_4(Mebta)_2]\}_n$ (**3**).

The crystal structure of $\mathbf{4} \cdot 0.25H_2O$ is composed of $[Cu_4OCl_6(Mebta)_4]$ molecules and water solvate molecules; the latter will not be further discussed. The molecule $[Cu_4OCl_6(Mebta)_4]$ consists of a tetrahedron of Cu^{II} atoms held together by one central μ_4-oxide ion and six μ-chloro ligands; each chloride spans an edge of the tetrahedron. One Mebta molecule is bound to each Cu^{II} atom in a terminal fashion. The μ_4-oxo group and two of the bridging chloro ligands [Cl(3), Cl(4)] lie on a twofold axis. The $Cu_4(\mu_4\text{-O})$ tetrahedron is almost regular, the Cu...Cu distances being between 3.103(4) and 3.152(3) Å, and the Cu–O–Cu angles varying from 108.6(1) to 110.9(2)°. The central $\mu_4\text{-}O^{2-}$ ligand is linked symmetrically to Cu^{II} ions, the individual bond lengths being 1.908(3) and 1.914(3) Å. The chloro bridges involving Cl(1) and Cl(2) [and their symmetry partners] are slightly asymmetrical, with Cu–Cl distances ranging from 2.378(2) to 2.449(2) Å ; the greatest asymmetry occurs for the Cu(1)–Cl(2)–Cu(2′) system. Angles at the bridging chloride ions are all acute, with individual values ranging from 80.0(1)° to 82.5(1)°.

The six chloro ligands comprise a rather distorted octahedron around the central oxide ion; the Cl...Cl, O...Cl distances and *cis* Cl...O...Cl angles vary as follows: O...Cl = 2.882(2)–2.953(2) Å, Cl...Cl = 3.982(3)–4.248(3) Å, Cl...O...Cl = 86.5(2)–93.5(2)°. These variations, however, are not as large as those observed in the structurally similar complexes $[Cu_4OCl_6(py)_4]$ (O...Cl = 2.92–2.96 Å, Cl...Cl = 3.93–4.41 Å, Cl...O... Cl = 84–98°) [39] and $[Cu_4OCl_6(2\text{-pic})_4]$ (O...Cl = 2.87–3.03 Å, Cl...Cl = 3.73–4.55 Å) [40], where inter- and intramolecular steric hindrances were postulated as reasons for the distortions in the chloride octahedron (py = pyridine, 2-pic = 2-methylpyridine).

Each of the Cu^{II} atoms is in a slightly distorted trigonal bipyramidal coordination environment, with the chloro ligands in the three equatorial sites. The Cu^{II} atoms are displaced out of the planes of their respective equatorial chlorides by 0.218(2) [Cu(1), Cu(1′)] and 0.212(3) [Cu(2), Cu(2′)] Å in the directions of the donor nitrogen atoms. The N–Cu–Cl angles range from 91.4(2) to 101.0(2)°, whereas the O–Cu–Cl angles are significantly smaller [83.5(1)–86.4(1)°]. The equatorial

Table 5
Comparison of selected structural parameters (Å, °) for $\{[Cu_2Cl_4(Mebta)_2]\}_n$ (**3**) and representative bis(μ-chloro) 1D copper(II) complexes of the general formula $\{[CuCl_2L_2]\}_n$ (L = monodentate ligand)

Compound[a]	Cu–Cl	Cu...Cu	Cu–Cl–Cu	Reference
$\{[CuCl_2(py)_2]\}_n$	3.026, 2.299	3.870	88.5	[35]
$\{[CuCl_2(4\text{-V-py})_2]\}_n$	3.100, 2.310	3.910	91.5	[36,37]
$\{[CuCl_2(4\text{-Et-py})_2]\}_n$	3.210, 2.280	4.000	91.9	[37]
$\{[CuCl_2(tz)_2]\}_n$	2.998, 2.322	3.853	91.9	[38]
$\{[Cu_2Cl_4(Mebta)_2]\}_n$	2.534, 2.261	3.556	95.6	this work

[a] *Abbreviations*: py, pyridine; 4-V-py, 4-vinylpyridine; 4-Et-py, 4-ethylpyridine; tz, triazole.

Table 6
Selected interatomic distances (Å) and angles (°) for complex $4 \cdot 0.25H_2O$

Cu(1)–Cl(1)	2.434(2)	Cl(1)...Cl(1′)	5.822(3)
Cu(1)–Cl(2)	2.378(2)	Cl(1)...Cl(2)	4.139(3)
Cu(1)–Cl(4)	2.370(2)	Cl(1)...Cl(2′)	4.176(3)
Cu(1)–N(3)	1.970(5)	Cl(1)...Cl(3)	4.223(3)
Cu(1)–O	1.908(3)	Cl(1)...Cl(4)	3.982(3)
Cu(2)–Cl(1)	2.372(2)	Cl(2)...Cl(2′)	5.897(3)
Cu(2)–Cl(2′)	2.449(2)	Cl(2)...Cl(3)	4.011(3)
Cu(2)–Cl(3)	2.390(2)	Cl(2)...Cl(4)	4.248(3)
Cu(2)–N(13)	1.985(5)	Cl(3)...Cl(4)	5.777(3)
Cu(2)–O	1.914(3)	Cu(1)...Cu(1′)	3.109(4)
Cl(1)...O	2.917(2)	Cu(1)...Cu(2)	3.127(3)
Cl(2)...O	2.953(2)	Cu(1)...Cu(2′)	3.103(4)
Cl(3)...O	2.882(2)	Cu(2)...Cu(2′)	3.152(3)
Cl(4)...O	2.895(2)		
Cl(1)–Cu(1)–Cl(2)	118.7(1)	Cu(1)–O–Cu(1′)	109.1(2)
Cl(1)–Cu(1)–Cl(4)	112.0(1)	Cu(1)–O–Cu(2)	109.8(1)
Cl(1)–Cu(1)–N(3)	94.0(2)	Cu(1)–O–Cu(2′)	108.6(1)
Cl(1)–Cu(1)–O	83.5(1)	Cu(2)–O–Cu(2′)	110.9(2)
Cl(2)–Cu(1)–Cl(4)	127.0(1)	Cu(1)–Cl(4)–Cu(1′)	82.0(1)
Cl(2)–Cu(1)–N(3)	94.3(2)	Cu(1)–Cl(1)–Cu(2)	81.2(1)
Cl(2)–Cu(1)–O	86.4(1)	Cu(1)–Cl(2)–Cu(2′)	80.0(1)
Cl(4)–Cu(1)–N(3)	97.2(2)	Cu(2)–Cl(3)–Cu(2′)	82.5(1)
Cl(4)–Cu(1)–O	84.4(1)	Cl(1)...O...Cl(1′)	173.0(1)
N(3)–Cu(1)–O	177.4(2)	Cl(1)...O...Cl(2)	89.7(2)
Cl(1)–Cu(2)–Cl(2′)	120.0(1)	Cl(1)...O...Cl(2′)	90.7(2)
Cl(1)–Cu(2)–Cl(3)	125.0(1)	Cl(1)...O...Cl(3)	93.5(2)
Cl(1)–Cu(2)–N(13)	91.4(2)	Cl(1)...O...Cl(4)	86.5(2)
Cl(1)–Cu(2)–O	85.1(1)	Cl(2)...O...Cl(2′)	173.7(3)
Cl(2′)–Cu(2)–Cl(3)	112.0(1)	Cl(2)...O...Cl(3)	86.8(4)
Cl(2′)–Cu(2)–N(13)	95.3(2)	Cl(2)...O...Cl(4)	93.2(4)
Cl(2′)–Cu(2)–O	84.3(1)	Cl(3)...O...Cl(4)	180.0(1)
Cl(3)–Cu(2)–N(13)	101.0(2)	N(1)–N(2)–N(3)	108.3(5)
Cl(3)–Cu(2)–O	83.3(1)	N(11)–N(12)–N(13)	108.0(5)
N(13)–Cu(2)–O	175.5(2)		

Symmetry code: $' = -x + 1/2, -y + 1/2, z$.

Cl–Cu–Cl angles vary from 112.0(1)° to 127.0(1)°, and the N–Cu–O angles are 177.4(2) and 175.5(2)° for Cu(1) and Cu(2), respectively.

Several structurally characterized examples of complexes containing the $[Cu_4^{II}(\mu_4\text{-}O)(\mu\text{-}X)_6]^0$ core (X = Cl, Br) are now available. Since Bertrand and Kelley [41] and tom Dieck and co-workers [42] characterized the first tetranuclear copper(II) complexes of the general formula $[Cu_4OX_{10-x}L_x]^{x-4}$, where L represents a monodentate ligand, a number of these compounds with the specific formula $[Cu_4OX_6L_4]$ have been synthesized. All these complexes have the same structural motif, with four Cu^{II} atoms at the corners of a tetrahedron around the central $\mu_4\text{-}O^{2-}$ group and six doubly bridging halogeno ions over each edge of the tetrahedron. In Table 7 are compared selected structural parameters for $4 \cdot 0.25H_2O$ and the representative complex $[Cu_4OCl_6(Hdmppz)_4]$, where Hdmppz is 3,4-dimethyl-5-phenylpyrazole [43]; the comparison reveals that the structural similarity between these complexes is impressive.

Table 7
Comparison of selected structural parameters (Å, °) for complex $[Cu_4OCl_6(Mebta)_4] \cdot 0.25H_2O$ ($4 \cdot 0.25H_2O$) and complex $[Cu_4OCl_6(Hdmppz)_4]$

Parameter	4	$[Cu_4OCl_6(Hdmppz)_4]$[a,b,c]
Cu...Cu	3.103–3.152	3.079–3.173
Cu–O	1.908, 1.913	1.905, 1.913
Cu–N	1.970, 1.985	1.960, 1.964
Cu–Cl	2.370–2.449	2.352–2.499
Cu–O–Cu	108.6–110.9	107.4–112.4
Cu–Cl–Cu	80.0–82.5	78.8–81.9
Cl–Cu–Cl[d]	112.0–127.0	118.0–121.3
N–Cu–O[e]	175.5, 177.4	175.8, 176.3

[a] *Abbreviation*: Hdmppz, 3, 4-dimethyl-5-phenylpyrazole.
[b] This cluster is also positioned on a twofold axis through two chlorides and the $\mu_4\text{-}O^{2-}$ group.
[c] Ref. [43].
[d] Equatorial angles in the tbp environments of the Cu^{II} atoms.
[e] Axial angles in the tbp environments of the Cu^{II} atoms.

Complex **5** crystallizes in the triclinic space group $P\bar{1}$ Its crystal structure consists of dinuclear $[Cu_2Cl_2(Mebta)_6]^{2+}$ cations and ClO_4^- counterions; the latter will not be further discussed. The two Cu^{II} centres are asymmetrically bridged by two chloro ligands; three monodentate Mebta molecules complete five-coordination at each metal. The bridging Cu_2Cl_2 unit is constrained to be planar by the presence of a crystallographic inversion centre in the middle of the dimer. The Cu–Cl bond lengths in this compound [2.327(1) and 2.554(1) Å] are comparable to the two bridging Cu–Cl bond lengths found in **1** [2.302(1) and 2.629(1) Å]. The Cu–N distances [2.001(2)–2.026(2) Å] are nearly identical to the values of 2.021(1) and 2.023(1) Å observed in **1**.

The five donor atoms within bonding distances do not define a regular polyhedron around copper. Analysis of the shape-determining angles using the approach of Reedijk and co-workers [44] yields a value for trigonality index, τ, of 0.5 ($\tau = 0$ and 1 for perfect square pyramidal and trigonal bipyramidal geometries, respectively). Thus, the geometry about Cu(1) [Cu(1′)] is significantly distorted and can be described as either distorted tbp or distorted sp. With use of the tbp description the axial sites of Cu(1) are occupied by N(23) and Cl(1′), with atoms N(3), N(13) and Cl(1) making up the equatorial plane. The equatorial bond angles are 103.1(1)°, 109.8(1)° and 147.0(1)°. The rather large steric hindrance caused by the size of the two "equatorial" Mebta can be one reason for the large N(3)–Cu(1)–N(13) angle of 147.0(1)°. For the sp description the basal plane would consist of the atoms N(3), N(13), N(23) and Cl(1′), with Cl(1) occupying the apical site.

The closest precedent to **5** is complex $[Cu_2(\mu\text{-}Cl)_2(dien)_2](ClO_4)_2$ [45], where dien is diethylenetriamine; in the latter each Cu^{II} atom is surrounded by

Table 8
Selected interatomic distances (Å) and angles (°) for complex **5**

Cu(1)–Cl(1)	2.554(1)	Cu(1)–N(13)	2.013(2)
Cu(1)–Cl(1′)	2.327(1)	Cu(1)–N(23)	2.026(2)
Cu(1)–N(3)	2.001(2)	Cu(1)...Cu(1′)	3.543(2)
Cl(1)–Cu(1)–Cl(1′)	87.1(1)	Cl(1′)–Cu(1)–N(23)	176.9(1)
Cl(1)–Cu(1)–N(3)	109.8(1)	N(3)–Cu(1)–N(13)	147.0(1)
Cl(1)–Cu(1)–N(13)	103.1(1)	N(3)–Cu(1)–N(23)	86.8(1)
Cl(1′)–Cu(1)–N(23)	94.4(1)	N(13)–Cu(1)–N(23)	92.7(1)
Cl(1′)–Cu(1)–N(3)	90.1(1)	Cu(1)–Cl(1)–Cu(1′)	92.9(1)
Cl(1′)–Cu(1)–N(13)	89.7(1)		

Symmetry code: ′ = $-x$, $-y+1$, $-z$.

the two bridging chlorides and three nitrogen atoms belonging to one tridentate chelating ligand in a distorted coordination environment [45].

3.3. IR, far-IR and electronic spectroscopy, and thermal decomposition data

Diagnostic IR, far-IR and solution electronic spectral data of complexes **1**–**5** are given in Table 9. The IR spectrum of free Mebta exhibits two bands at 1197 and 1110 cm^{-1} associated with the ν(N=N) and ν(N–N) modes of vibration, respectively [3,5]. These bands are shifted to 1220–1230 and ~1140 cm^{-1}, respectively, in the spectra of the complexes. These shifts are compatible with N(3) being the donor atom to copper(II) [3,5]. The coordinated Mebta is considered responsible for the two bands at ~780 and 750 cm^{-1} in **2**–**5**; the latter is stronger and assigned as a C–H out-of-plane vibration and the former is due to a vibration involving both benzene and triazole in-plane bending [10]. These modes coincide at 759 cm^{-1} in the spectrum of **1**. The spectrum of **5** exhibits strong bands at 1100 and 630 cm^{-1} due to the $\nu_3(F_2)[\nu_d(Cl–O)]$ and $\nu_4(F_2)[\delta_d(OClO)]$ of the uncoordinated ClO_4^- [46].

Assignments of metal–ligand stretching vibrations in Table 9 have been carefully given by consideration of the frequencies of the internal modes of Mebta and studying literature reports [11,40,46]. The spectrum of **4** · 0.25H_2O shows a strong IR absorption at 575 cm^{-1}, characteristic of the asymmetric vibration (F_2 mode) of the $[Cu_4(\mu_4\text{-}O)]^{6+}$ core [40]. The non-appearance of ν(Cu–Cl) bands above 235 cm^{-1} in **3**–**5** is consistent with their structures which contain exclusively bridging chlorides [11]. The terminal and bridging Cu–Cl stretching vibrations in **1** appear at 299, 180, and 162 cm^{-1}, respectively [11,46]. The $\nu(Cu–N_{Mebta})$ vibrations appear between 287 and 265 cm^{-1}.

From the solution electronic spectra, it is difficult to decide if the structures seen in the solid state persist in solution; structural changes are possible in solvents of high donor capacity (MeOH, DMF). The UV bands are due to ligand-to-metal charge transfer transitions [40,43], while a d–d transition is seen in the 11.50–12.60 kK range [11,40,43]. The electronic spectrum of **4** · 0.25H_2O in MeCN is fairly similar to the solid-state spectrum of the structurally similar cluster $[Cu_4OCl_6(Hdmppz)_4]$ [43].

TG, DTG and DTA data are available for complexes **1**, **3**, **4** · 0.25H_2O and **5**. The first decomposition steps (30–215 °C) of **1** have already been described in part 2.3.3. The intermediate formed (proved to be complex **3**, see Section 3.1) decomposes in two successive, endothermic steps between 215 and 295 °C

Table 9
Diagnostic IR, far-IR and electronic spectroscopic data[a] for complexes **1**–**5**

Assignment	**1**	**2**	**3**	**4** · 0.25H_2O	**5**
IR/far-IR (cm^{-1})					
ν(N=N)	1230 s	1222 s	1225 s	1230 s	1230 s
ν(N–N)	1140 m	1132 m	1141 m	1141 w, 1125 w	1146 s
$\nu_3(ClO_4^-)$					~1100 sb
$\nu_4(ClO_4^-)$					630 s
ν(Cu–O)				575 s	
$\nu(Cu–Cl)_t$	299 sb	[b]			
$\nu(CuCl)_b$	180 m, 162 s		175 sh[c], 159 s	231 s[c], 191 w	188 m, 167 s
ν(Cu–N)	271 sh, 265 m	[b]	287 s	274 m	275 sb
UV/VIS (kK)					
LMCT	26.52[d]	24.31[d]	30.95[e], 22.95[e]	27.40 sh[f]	27.02[e]
d–d	12.31[d]	11.50[d]	~12.50[e]	12.60[f]	12.20[e]

[a] *Abbreviations*: b, broad; LMCT, ligand-to-metal charge transfer; m, medium; $\nu(CuCl)_b$, stretching frequency of the bridging Cl–Cl bond; $\nu(Cu–Cl)_t$, stretching frequency of the terminal Cu–Cl bond; b, broad; m, medium; s, strong; sh, shoulder; w, weak.
[b] No far-IR data are available for this complex.
[c] Possibly overlapping with a vibration of Mebta.
[d] In MeOH.
[e] In DMF.
[f] In MeCN.

according to Eq. (9). Weight loss calculations indicate that the final residue at 600 °C is CuO. Complex **3** is thermally stable up to 215 °C; its decomposition pattern above 215 °C is almost identical with that of the intermediate obtained from the decomposition of **1** at 205–215 °C, as expected.

$$\{[Cu_2Cl_4(Mebta)_2]\}_n \xrightarrow[N_2]{215-295^\circ C} 2nCuCl_2 + 2nMebta\uparrow \quad (9)$$

Complex $\mathbf{4}\cdot 0.25H_2O$ decomposes endothermically between room temperature and 440 °C according to the tentative scheme described by Eq. (10). The pattern above this temperature is rather simple involving slight increase of weight (possibly due to slow oxidation). A strong endothermic DTA peak at 550 °C, not accompanied by a weight change, may be due to partial melting or to a phase transition. The unstable stoichiometric compounds in the 84–440 °C range could not be isolated by the temperature arrest technique in a nitrogen atmosphere due to the absence of well-defined plateaux in the TG curve (even at low heating rates).

$$[Cu_4OCl_6(Mebta)_4]\cdot 0.25H_2O \xrightarrow[N_2]{30-60^\circ C} [Cu_4OCl_6(Mebta)_4] \xrightarrow[N_2]{84-266^\circ C} [Cu_4OCl_6(Mebta)] \xrightarrow[N_2]{267-305^\circ C} Cu_4^{I/II}OCl_5 \xrightarrow[N_2]{307-440^\circ C} Cu_4^{I}OCl_2 \quad (10)$$

Contrary to our expectations, complex **5** does not explode at high temperatures. The compound is stable in the 30–175 °C range. The inflections in the TG curve and the large number of DTG peaks above 175 °C indicates a complex thermal decomposition with overlapping degradation processes. The absence of TG plateaux indicate that stable intermediates cannot be formed. No stoichiometric compounds could be assigned to the TG curve's inflections. The final residue at 600 °C appears to be CuO.

3.4. Magnetic and EPR studies of complexes *1*, *3* and *5*

Variable-temperature magnetic susceptibility (χ_M) data were collected for powdered samples of **1**, **3** and **5** in the temperature range 4.2–296 K.

Data for **1** are shown in Fig. 7. The product $\chi_M T$ increases upon cooling, from 0.417 cm^3 K mol^{-1} at 294 K to 0.454 cm^3 K mol^{-1} at 4.2 K, which, together with the positive Weiss temperature ($\theta = +0.3$ K and $\theta = +3.1$ K in the 4.2–294 K and 50–294 K temperature ranges, respectively), is consistent with intramolecular ferromagnetic coupling. Hence, the experimental data between 4.2 and 294 K have been fitted to the Bleaney–Bowers equation [47] with a molecular-field correction [48], namely:

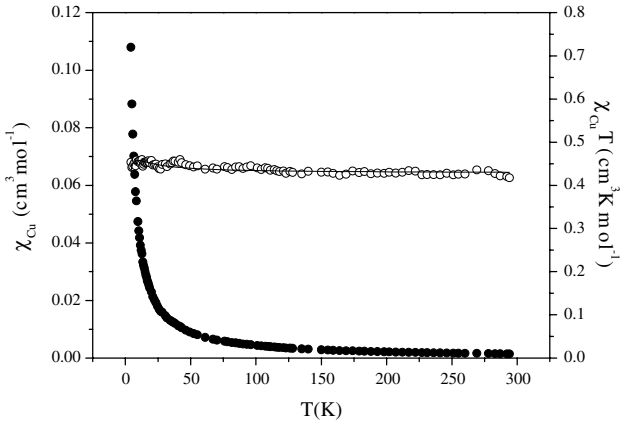

Fig. 7. Plot of χ_M (•) and $\chi_M T$ (○) vs T for complex **1**. The solid line results from a least-squares fit of the data to the theoretical model; see text for fitting parameters.

$$\chi_M^{corr} = \frac{\chi_M}{\frac{1-2zJ'\chi_M}{N\beta^2\langle g\rangle^2}}, \quad (11)$$

where,

$$\chi_M = \frac{N\beta^2\langle g\rangle^2}{3kT}[1 + 1/3e^{-2J/kT}]^{-1}, \quad (12)$$

$\langle g\rangle$ is the average splitting factor obtained from the fitting procedure, z is the number of the nearest neighbouring dimers in the crystal lattice, J' is the interdimer exchange parameter, while the other symbols have their usual meaning. The best fitting parameters obtained are $2J = +6.7$ cm^{-1} and $zJ' = -1.2$ cm^{-1} and $\langle g\rangle = 2.137$ by minimizing the function R [Eq. (13)] to 4.46×10^{-3}.

$$R = \sqrt{\frac{\sum_{i=1}^{n}[(\chi_M)_i^{exp} - (\chi_M)_i^{calc}]^2/(\chi_M)_i^{exp^2}}{\sum_{i=1}^{n}1/[(\chi_M)_i^{exp}]^2}} \quad (13)$$

The X-band EPR spectrum of a powdered sample of **1** is axial ($g_\parallel = 2.210$, $g_\perp = 2.078$, $\langle g\rangle = 2.123$) and remains unchanged in the 77–300 K temperature range.

Complex **5** exhibits a very similar magnetic and EPR behaviour with that of **1** (Fig. 8). Upon cooling, the product $\chi_M T$ increases, reaches a maximum of 0.546 cm^3 K mol^{-1} at 4.2 K which, along with the positive Curie–Weiss temperature ($\theta = +0.9$ K in the 4.2–296 K and $\theta = +4.2$ K in the 50–296 K range), is indicative of intramolecular ferromagnetic interaction. Consequently, we used the same exchange Hamiltonian and the susceptibility expressions provided by Eqs. (11) and (12) as for **1**. The experimental magnetic susceptibility data in the 4.2–296 K range were least-squares fitted to Eq. (11) to give the parameters $2J = +10.4$ cm^{-1}, $zJ' = -0.5$ cm^{-1} and $\langle g\rangle = 2.187$ by minimizing the factor R [Eq. (13)] to 5.52×10^{-3}.

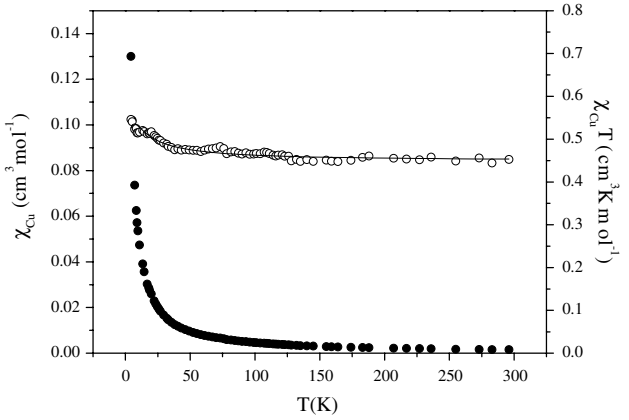

Fig. 8. Plot of χ_M (•) and $\chi_M T$ (○) vs T for complex **5**. The solid line results from a least-squares fit of the data to the theoretical model; see text for fitting parameters.

The X-band EPR spectrum of a powdered sample of **1** is also axial ($g_\parallel = 2.321$, $g_\perp = 2.043$, $\langle g \rangle = 2.140$) and remains unchanged in the 77–300 K temperature range.

For complex **3**, the product $\chi_M T$ (Fig. 9) increases upon cooling, reaches a maximum of 0.621 cm^3 K mol^{-1} at ca. 20 K and then decreases to 0.563 cm^3 K mol^{-1} at 4.3 K. The compound follows the Curie–Weiss law, $\chi_{Cu} = 0.471/(T - 12.4)$, in the higher temperature range ($T > 50$ K). Taking into account the crystal structure of the complex (see above), the magnetic data were fitted to the Heisenberg model of the magnetic interaction (Padé expansion series [49–51] for $S = 1/2$) assuming a first-order molecular-field correction to account for the interchain interactions. The analytical expression for the susceptibility is given by Eq. (14):

$$\chi_M^{corr} = \frac{\chi_C}{\frac{1-2zJ'\chi_C}{N\beta^2 g^2}}. \tag{14}$$

The term χ_C is the susceptibility of a Heisenberg chain given by Eq. (15):

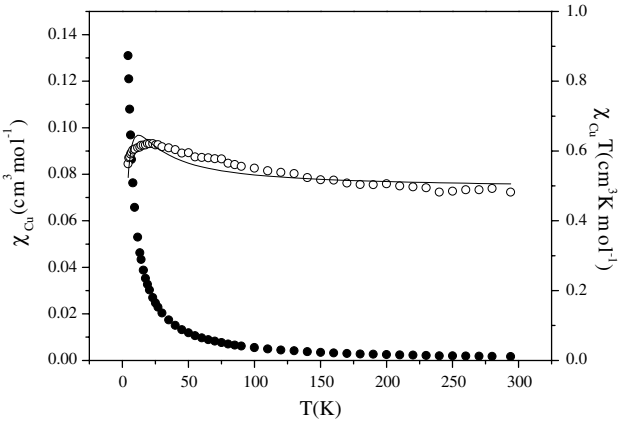

Fig. 9. Plot of χ_M (•) and $\chi_M T$ (○) vs T for complex **3**. The solid line was calculated with the parameters reported in the text.

$$\chi_C = \frac{N\beta^2 g^2}{4kT}\left(\frac{L}{M}\right)^{2/3}, \tag{15}$$

where,

$$L = 1 + 5.7979916K + 16.902653K^2 + 29.376855K^3 + 29.832959K^4 + 14.036918K^5,$$

$$M = 1 + 2.7979916K + 7.0086780K^2 + 8.6538644K^3 + 4.5743114K^4, \quad K = J/2kT,$$

z is the number of the nearest neighbouring chains, J' is the interchain exchange parameter, and g is the spectroscopic splitting parameter. The best fitting parameters obtained are $J = +7.8$ cm^{-1} and $zJ' = -3.5$ cm^{-1} and $g = 2.290$ with an R value [Eq. (13)] of 1.38×10^{-4}. Consequently, complex **3** constitutes an interesting example of a molecular ferromagnet in which chains are coupled antiferromagnetically.

The X-band EPR spectrum of a powdered sample of **3** is isotropic in the whole temperature range (4.2–293 K). The peak to peak linewidth of the signal increases upon cooling ($\delta H_{pp} = 290$, 355 and 477 G at 293, 77 and 4.2 K, respectively). Spectroscopic splitting parameter value taken from the EPR spectra of the complex is 2.15.

3.5. Quantum-chemical interpretation of the exchange coupling for complexes *1* and *5*

First of all it is important to emphasize that the positive values of $2J$ for complexes **1** and **5** are the highest yet reported for a member of this class of bis(μ-chloro) copper(II) dimers (Table 10).

It was shown in Section 3.2 that the Cu^{II} atoms in **1** are in regular square-pyramidal surroundings, whereas the coordination polyhedron in **5** can be characterized as intermediate between a trigonal bipyramid and a square pyramid ($\tau = 0.5$ [44]). Consequently, **1** belongs to the square-pyramidal apical-basal type **I** (Scheme 1), while **5** may be considered as a trigonal bipyramidal axial-equatorial dimer of type **II** (Scheme 1). It is well-known that in the type-**I** and -**II** geometries, the unpaired electron lies predominantly in a $|x^2 - y^2\rangle$- and a $|z^2|$-type orbital, respectively. Hatfield and coworkers have shown [18] that this distinction is unnecessary for the two types, since they are interconvertible by a single angular deformation (of a kind of the Berry mechanism for intramolecular rearrangement). Thus, electronically the observed dimers of types **I** and **II** are substantially similar and, in fact, the tbp (type **II**) complexes exhibit a predominantly $|x^2 - y^2\rangle$ ground state [18,60] as expected for sp geometry; consequently, all complexes in Table 10 may be viewed as belonging to the same structural type and their magnetic properties can be compared directly [18].

As already stated in Section 1, a strong correlation has been found [18] between the singlet–triplet splitting

Table 10
Structural and magnetic data of structurally characterized bis(μ-chloro) copper(II) dimers [a]

Numbering	Complex[b]	$2J$ (cm^{-1})	R (Å)	Cu–Cl (Å)	φ (deg)	φ/R (deg $Å^{-1}$)	ω (deg)	Type[d]	Reference
1	$[Cu_2Cl_4L_2]$	4.9	2.84	2.27	96.7	34.0	n.a.[c]	**I**	[52]
2	$[Cu_2Cl_4(dmgH)_2]$	6.3	2.70	2.24	88.0	32.6	88.0	**I**	[18,32,53]
3	$[Cu_2Cl_4(Mebta)_4]$ (**1**)	6.7	2.63	2.30	88.1	33.5	90.1	**I**	this work
4	$[Cu_2Cl_4(dmen)_2]$	−2.1	2.73	2.31	86.1	31.5	84.1	**I**	[31]
5	$[Cu_2Cl_2(Pypep)_2]$	−4.6	2.83	2.32	91.1	32.2	91.5	**I**	[54]
6	$[Cu_2Cl_4(tmen)_2]$	−5.6	3.15	2.26	96.8	30.8	85.3	**I**	[55]
7	$[Cu_2Cl_2(terpy)_2]^{2+}$	−5.9	2.72	2.22	90.1	33.0	81.0	**I**	[56]
8	$[Cu_2Cl_4(2\text{-pic})_4]$	−7.4	3.36	2.29	100.6	29.9	94.0	**I**	[32]
9	$[Cu_2\ Cl_4\ (L–L)_2]$	−10.0	2.47	2.27	95.7	38.7	79.7	**I**	[33]
10	$[Cu_2Cl_4(Et_3\ en)_2]$	0.1	2.73	2.28	94.8	34.8	111.0	**II**	[18]
11	$[Cu_2Cl_3(L'H)_5]Cl$	5.6	2.62	2.40	89.0	33.9	124.4	**II**	[57]
12	$[Cu_2Cl_2(Mebta)_6]^{2+}$ (**5**)	10.4	2.55	2.33	92.9	36.4	94.5	**II**	this work
13	$[Cu_2Cl_8]^{4-}$	−14.6	2.70	2.32	95.2	35.2	118.3	**II**	[58,60]
14	$[Cu_2Cl_6(GuaH)_2]$	−82.6	2.45	2.29	97.9	40.0	114.0	**II**	[18,59]

[a] See text and Scheme 2 for definition of the various parameters.
[b] *Abbreviations*: dmen, *N*,*N*-dimethylethylenediamine; dmgH, dimethylglyoxime; Et_3en, *N*,*N*,*N*′-triethylethylenediamine, GuaH, the guaninium cation; L, 2,2-bis-(2-pyridyl)-1,3-dioxolane, L–L, 2-(2′-pyridyl)quinoxaline; L′H, benzimidazole; Mebta, 1-methylbenzotriazole; 2-pic, 2-methylpyridine; Pypep, the monoanion of *N*-(2-(4-imidazolyl)ethyl)pyridine-2-carboxamide; terpy, 2,2′:6′,2″-terpyridine; tmen, *N*,*N*,*N*′,*N*′-tetramethylethylenediamine.
[c] Not available.
[d] See Scheme 1.

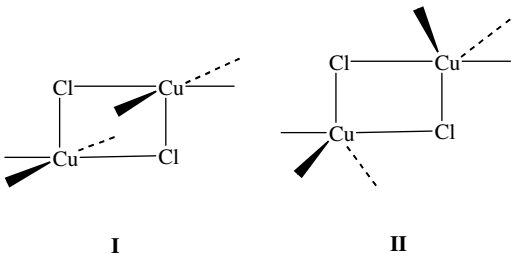

Scheme 1. The two common structural types of the bis(μ-chloro) copper(II) dimers: square-pyramidal apical-basal dimers (**I**) and trigonal-bipyramidal axial-equatorial dimers (**II**).

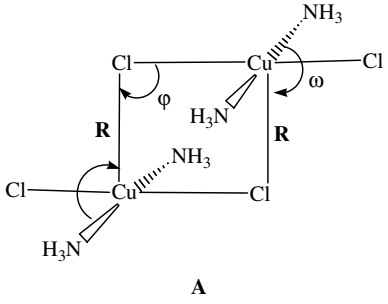

Scheme 2. The model dinuclear complex $[Cu_2Cl_4(NH_3)_4]$ (**A**) used for the EHMO calculations; see text for more details.

($2J$) and the quotient φ/R in the five-coordinate $[Cu_2(\mu\text{-}Cl)_2Cl_2L_4]$ and $[Cu_2(\mu\text{-}Cl)_2Cl_2(L–L)_2]$ complexes (L = monodentate ligand, L–L = bidentate chelating ligand), where φ is the Cu–Cl–Cu′ bridging angle and R is the longest bridging bond distance; the latter is the axial Cu–Cl bridging distance in **I** and the equatorial distance in **II**. In complex **1** a mean φ/R value of 33.5 deg $Å^{-1}$ is deduced, for which the empirical correlation predicts a ferromagnetic interaction with a $2J$ value of ca. +5 cm^{-1}, in good agreement with the observed one of +6.7 cm^{-1}. However, complex **5** has a φ/R value of 36.4 deg $Å^{-1}$, for which the empirical correlation predicts [18] an antiferromagnetic interaction with a $2J$ value of ca. −23 cm^{-1}. This value is in profound contradiction to the experimental one ($2J$ = +10.4 cm^{-1}). In an attempt to investigate this discrepancy, and since type **II** dimers can be derived from type **I** dimers (by varying the ω angle – being the dihedral N–Cu–Cl one – in Scheme 2 from 90° to 120°), EHMO calculations were performed on the general model complex **A** shown in Scheme 2. The choice of the model system **A** was based on the fact that, in the present case, the three major structural factors governing the exchange interaction are the φ and ω angles, and the R bond distance. For the study of the φ, R dependence of the $\varepsilon_A - \varepsilon_S = \delta$ difference, where δ denotes the energy difference between the symmetric and antisymmetric MOs of the Cl^- bridging ligand (symmetry-adapted to interact with the degenerate singly occupied in- and out-of-phase combinations of the Cu d orbitals), most bond lengths (Cu–N = 2.0 Å, Cu–Cl = 2.30 Å, and N–H = 1.09 Å) of the model system were fixed as φ and R were varied from 85° to 105° and 2.20 to 3.50 Å, respectively. However, for the study of the ω, φ dependence of the $\varepsilon_A - \varepsilon_S = \delta$ difference, the Cu–Cl and R bond lengths were fixed at 2.30 and 2.84 Å (the latter being the corresponding mean experimental value), respectively; still, the ω and φ values were varied from 90° to 120° and 80° to 115°, respectively, and, hence, the φ/R values were varied from 28 to 40 deg $Å^{-1}$.

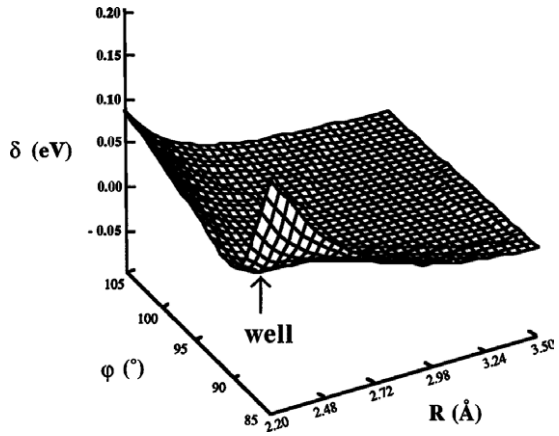

Fig. 10. 3D plot of the φ, R dependence of δ.

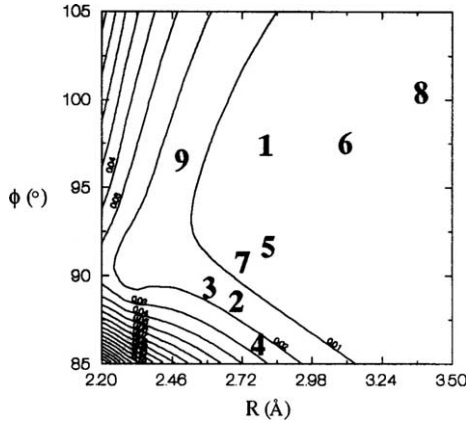

Fig. 11. Contour plot of the φ, R dependence of δ, including the type **I** complexes (see also Scheme 1) according to their (φ, R) values.

A 3D drawing of the φ, R dependence of δ is shown in Fig. 10; a contour plot of the same dependence is provided in Fig. 11. It is clear from both figures that there is a well-corresponding to the crossover point ($\delta = 0$), hence to ferromagnetic behaviour – at the φ and R pair values of 90° and 2.33 Å, respectively. The right part of the contour map exhibits a weak antiferromagnetic character, whereas its upper and lower left parts sharply exhibit its strong antiferromagnetic behaviour.

Moreover, Table 10 gives the experimental magnetic and structural data for some structurally characterized copper(II) dimers of both **I** and **II** types (Scheme 1). First, type **I** complexes are given in ascending order of their exchange parameters (numbering from 1 to 9), and then type **II** ones also in ascending order of their exchange parameters (numbering from 10 to 14). An inspection of the data presented in Table 10 clearly shows that, for both types **I** and **II** complexes, there are three compounds exhibiting weak ferromagnetic interaction.

In Fig. 11, the type **I** complexes are also shown according to their (φ,R)-pair values. It is clear from Fig. 11 that both ferromagnetic complexes with the numbers 2 and 3 (ours **1**) [see also Table 10] are arranged closer to the lower δ values of the well. Due to its lower R value (both complexes have practically the same φ value), the latter exhibits stronger ferromagnetism and lies closer to the well than the former. In a subsequent stage, all the rest antiferromagnetic type **I** complexes given in Table 10 are displayed according to their (φ, R) values. They are spread to the right of the previous complexes, corresponding to areas of the well with medium δ values. All these, in turn, further verify the significance of the two structural parameters φ and R in the enhancement of both ferromagnetic and antiferromagnetic interactions, and make them our favourite parameters for the establishment of a magnetostructural criterion. According to Fig. 11, one should expect that ferromagnetic interactions do occur close to the well of the figure, while antiferromagnetic ones do occur at areas on the right side exhibiting higher δ values. It is worthwhile mentioning at this point that the criterion just derived holds for neutral, type **I** $Cu(\mu\text{-}Cl)_2Cu$ moiety configurations involving two CuN_2Cl_3 square pyramids with parallel $CuN_2(\mu\text{-}Cl)Cl$ bases. However, Fig. 11 in conjunction with values in Table 10 also shows that, with the only exception of complex 1, the criterion holds for type **I** complexes irrespective of the type of their coordination sphere (CuN_2Cl_3 and/or CuN_3Cl_2).

A 3D drawing of the ω, φ dependence of δ is shown in Fig. 12; a contour plot of the same dependence is provided in Fig. 13. It becomes clear from both figures that there is a valley, the well of which – corresponding to the crossover point ($\delta = 0$), hence to ferromagnetic

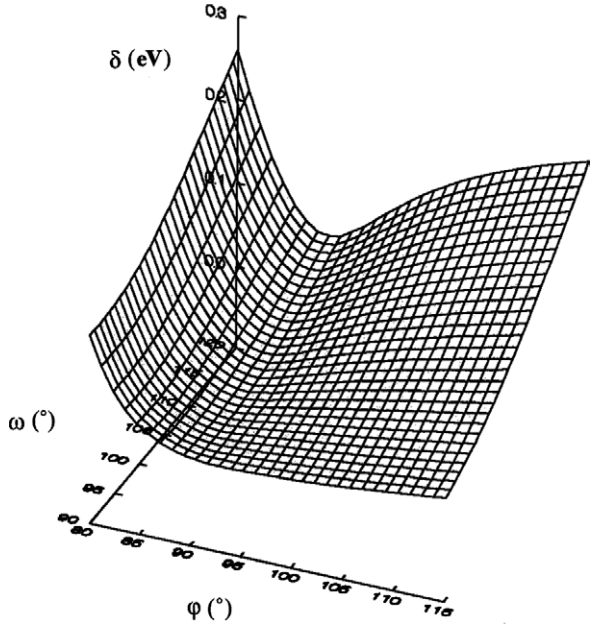

Fig. 12. 3D plot of the ω, φ dependence of δ.

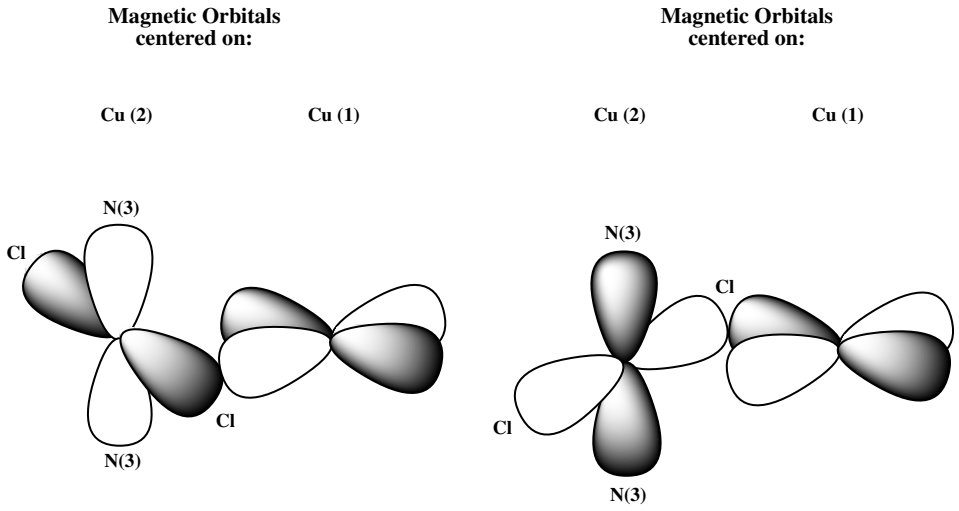

Scheme 3. Accidental orthogonality of the sequential magnetic orbitals in **3**, accounting for its intrachain ferromagnetic exchange interaction.

behaviour – corresponds to the ω and φ pair values of 120° and 90°, respectively; this valley proceeds parallel to the ω axis. The left part of the contour map strongly exhibits the antiferromagnetic character and this is also the case with the upper right part. The most crucial point emerging from both figures is that the slope of the antiferromagnetic region on the lower right part of the contour plot becomes less sharper upon bending of the ω angle from 90° to ca. 100°.

In Fig. 13, the type **II** complexes are also shown according to their (ω, φ)-pair values. It is clear from Fig. 13 that all three ferromagnetic complexes with the numbers 10, 11 and 12 (ours **5**) [see also Table 10] are arranged closer to the lower δ values of the well than the two antiferromagnetic ones. Complex 11 is not shown in Fig. 13, because it is arranged outside it, in the projection of the valley of the well. However, complex **5** (number 12 in Fig. 13 and Table 10) is arranged very close to the well. Both antiferromagnetic complexes 13 and 14 are arranged to the right of the three ferromagnetic ones, in areas of the well with the sharper slope of the antiferromagnetic region. All these, in turn, further verify the significance of ω and φ in the enhancement of both ferromagnetic and antiferromagnetic interactions making them serious candidates for the establishment of a magnetostructural criterion. According to Fig. 13, one should expect that *ferromagnetic interactions do occur close to the valley of the well of the figure*, *while antiferromagnetic ones do occur at areas on both left and upper right hill sides exhibiting higher δ values*. It should be stressed at this point that the criterion just derived holds (i) for neutral, type **II** Cu(μ-Cl)$_2$Cu moiety configurations involving two significantly distorted CuN_2Cl_3 trigonal bipyramids, and (ii) for type **II** complexes irrespective of their coordination sphere (CuN_2Cl_3, CuN_3Cl_2, $CuNCl_4$, and $CuCl_5$) and their total charge.

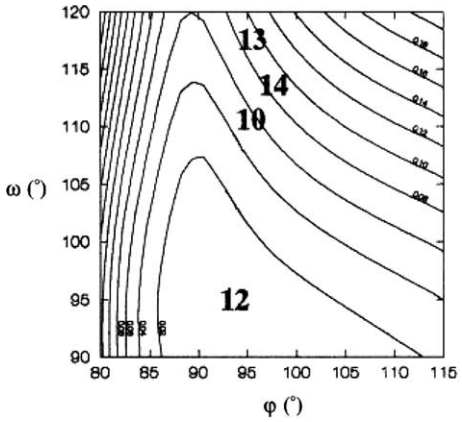

Fig. 13. Contour plot of the ω, φ dependence of δ, including the type **II** complexes (see also Scheme 1) according to their (ω, φ) values.

*3.6. Orbital interpretation of the exchange mechanism in complex **3***

Contrary to complexes **1** and **5**, complex **3** consists of well-separated linear chains possessing alternating square planar Cu(1)Cl$_4$ and *trans* octahedral Cu(2)Cl$_4$N$_2$ chromophores. The magnetic orbital in the former is a d-type orbital pointing towards the four nearest neighbours, i.e., four chloro ligands. This magnetic orbital is almost perpendicular to that centred on Cu(2) [dihedral angle of 89.4°]. However, the latter magnetic orbital, due to the four identical Cu(2)–Cl bond distances [2.534(1) Å] and the two identical, significantly shorter Cu(2)–N(3) bond distances [1.986(2) Å], could be either one of the two perpendicular (to each other) d-type orbital in the Cu(2)Cl$_2$N(3)$_2$ planes, see Scheme 3. Hence, the two sequential magnetic orbitals of Cu(1) and Cu(2) along each chain are accidentally orthogonal [51] to each other. This could account well for the ferromagnetic exchange interaction found experimentally.

4. Conclusions

Our systematic investigation of the $CuCl_2$/Mebta reaction system has confirmed our belief that a variety of complexes with interesting structures and properties are capable of existence. Suitable preparative procedures have now been developed, and the precise identity of the products has been shown to be dependent on the Cu^{II}:Mebta reaction ratio, the nature of the solvent and the absence/presence of counterions in the reaction systems. Such considerations will be important as this work is extended to other benzotriazole ligands.

It is interesting to compare the $CuCl_2$/Mebta and $CuBr_2$/Mebta [3] reaction systems. Although we do not claim that the synthetic investigations of these systems are complete, it seems that (i) for compounds $[CuX_2(Mebta)_2]$ and (possibly) the 1:1 CuX_2/Mebta complexes, the structures remain unchanged by halide substitution, (ii) complexes $[Cu_2Cl_4(Mebta)_4]$ (**1**), $[Cu_4OCl_6(Mebta)_4] \cdot 0.25H_2O$ (**4** · $0.25H_2O$) and $[Cu_2Cl_2(Mebta)_6](ClO_4)_2$ (**5**) have no known counterparts in $CuBr_2$/Mebta chemistry, and (iii) the mononuclear 1:3 bromo complex $[CuBr_2(Mebta)_3]$ [3] does not have its analogue in $CuCl_2$/Mebta chemistry. Electronic factors may be responsible for (ii) and (iii).

From the molecular magnetism viewpoint, complexes **1**, **3** and **5** are interesting because they exhibit intramolecular (**1**,**5**) and intrachain (**3**) ferromagnetic exchange interactions. We also believe that an important contribution of this work is the fact that insight concerning the effect of structural parameters on the sign and magnitude of the magnetic exchange interactions in **1** and **5** was gained through EHMO calculations performed on a model system. Calculations have permitted the establishment of a new criterion, holding for the magneto-structural correlations in bis(μ-chloro) copper(II) dimers.

5. Supplementary material

Crystallographic data (excluding structure factors) for the structures reported in this paper have been deposited with the Cambridge Crystallographic Data Centre, CCDC Nos. 237022(**1**), 237023(**2**), 237024(**3**), 237025(**4** · $0.25H_2O$) and 237026(**5**). Copies of this information may be obtained free of charge from the Director, CCDC, 12 Union Road, Cambridge CB2 1EZ, UK (fax: +44-1223-336-033; e-mail: deposit@ccdc.cam.ac.uk or ⟨www.ccdc.cam.ac.uk⟩).

Acknowledgements

The authors gratefully acknowledge the Greek General Secretariat of Research and Technology, the Research Committee of the University of Patras and the Polish Ministry of Science and Computerization (Grant 4T09A 11523) for support of this work.

References

[1] E. Diamantopoulou, C.P. Raptopoulou, A. Terzis, V. Tangoulis, S.P. Perlepes, Polyhedron 21 (2002) 2117, and references therein.
[2] V. Tangoulis, C.P. Raptopoulou, V. Psycharis, A. Terzis, K. Skorda, S.P. Perlepes, O. Cador, O. Kahn, E.G. Bakalbassis, Inorg. Chem. 39 (2000) 2522.
[3] K. Skorda, R. Keuleers, A. Terzis, C.P. Raptopoulou, S.P. Perlepes, J.C. Plakatouras, Polyhedron 18 (1999) 3067, and references therein.
[4] V. Tangoulis, C.P. Raptopoulou, A. Terzis, E.G. Bakalbassis, E. Diamantopoulou, S.P. Perlepes, Inorg. Chem. 37 (1998) 3145.
[5] J.C. Plakatouras, S.P. Perlepes, D. Mentzafos, A. Terzis, T. Bakas, V. Papaefthymiou, Polyhedron 11 (1992) 2657.
[6] W. Qafsaoui, Ch. Blanc, J. Roques, N. Pebere, A. Srhiri, C. Mijoule, G. Mankowski, J. Appl. Electrochem. 31 (2001) 223, and references therein.
[7] D. Sockalingum, M. Fleischmann, M. Musiani, Spectrochim. Acta 47A (1991) 1475, and references therein.
[8] B.-S. Fang, C.G. Olson, D.W. Lynch, Surf. Sci. 176 (1986) 476, and references therein.
[9] D. Chadwick, T. Hashemi, Corros. Sci. 18 (1978) 39.
[10] M. Murrie, D. Collison, C.D. Garner, M. Helliwell, P.A. Tasker, S.S. Turner, Polyhedron 17 (1998) 3031.
[11] J. Reedijk, A.R. Siedle, R.A. Velapoldi, J.A.M. Van Hest, Inorg. Chim. Acta 74 (1983) 109.
[12] R.E.P. Winpenny, J. Chem. Soc., Dalton Trans. (2002) 1.
[13] D. Gatteschi, R. Sessoli, Angew. Chem., Int. Ed. 42 (2003) 268.
[14] E.K. Brechin, C. Boskovic, W. Wernsdorfer, J. Yoo, A. Yamaguchi, E.C. Sanudo, T.R. Concolino, A.L. Rheingold, H. Ishimoto, D.N. Hendrickson, G. Christou, J. Am. Chem. Soc. 124 (2002) 9710.
[15] V. Tangoulis, E. Diamantopoulou, E.G. Bakalbassis, C.P. Raptopoulou, A. Terzis, S.P. Perlepes, Mol. Cryst. Liq. Cryst. 335 (1999) 463.
[16] L.F. Jones, E.K. Brechin, D. Collison, A. Harrison, S.J. Teat, W. Wernsdorfer, Chem. Commun. (2002) 2974.
[17] L.F. Jones, E.K. Brechin, D. Collison, J. Raftery, S.J. Teat, Inorg. Chem. 42 (2003) 6971.
[18] W.E. Marsh, K.C. Patel, W.E. Hatfield, D.J. Hodgson, Inorg. Chem. 22 (1983) 511, and references therein.
[19] C.P. Landee, R.E. Greeney, Inorg. Chem. 25 (1986) 3771.
[20] M.A. Romero, J.M. Salas, M. Quiros, M.P. Sanchez, J. Romero, D. Martin, Inorg. Chem. 33 (1994) 5477.
[21] K. Skorda, E.G. Bakalbassis, J. Mrozinski, S.P. Perlepes, C.P. Raptopoulou, A. Terzis, J. Chem. Soc., Dalton Trans. (1995) 2317.
[22] P.J. Hay, J.C. Thibeault, R. Hoffmann, J. Am. Chem. Soc. 97 (1975) 4884, and references therein.
[23] R. Hoffmann, J. Chem. Phys. 39 (1963) 1397.
[24] R. Hoffmann, W.N. Lipscomb, J. Chem. Phys. 36 (1962) 3179.
[25] R. Hoffmann, W.N. Lipscomb, J. Chem. Phys. 37 (1962) 2872.
[26] Th.C. Anaxagorou, G.A. Katsoulos, M.P. Sigalas, C.A. Tsipis, QCPE Bull. 14 (1994) 5.
[27] M. Wolfsberg, L. Helmholz, J. Chem. Phys. 20 (1952) 837.
[28] G.M. Sheldrick, SHELXS-86, Structure Solving Program, University of Göttingen, Göttingen, Germany, 1986.
[29] G.M. Sheldrick, SHELXL-97, Program for the Refinement of Crystal Structures from Diffraction Data, University of Göttingen, Göttingen, Germany, 1997.
[30] W.E. Hatfield, Comments Inorg. Chem. 1 (1981) 105.

[31] D.W. Phelps, W.H. Goodman, D.J. Hodgson, Inorg. Chem. 15 (1976) 2266.
[32] W.E. Marsh, W.E. Hatfield, D.J. Hodgson, Inorg. Chem. 21 (1982) 2679, and references therein.
[33] E.G. Bakalbassis, J. Mrozinski, S.P. Perlepes, N. Hadjiliadis, F. Lianza, A. Albinati, Polyhedron 13 (1994) 3209, and references therein.
[34] J.A.G. van Ooijen, J. Reedijk, A.L. Spek, J. Chem. Soc., Dalton Trans. (1979) 1183.
[35] B. Morosin, Acta Crystallogr., Sect. B 31 (1975) 632.
[36] M. Laing, E. Horsfield, J. Chem. Soc., Chem. Commun. (1968) 735.
[37] V.H. Crawford, W.E. Hatfield, Inorg. Chem. 16 (1977) 1336.
[38] W.E. Estes, D.P. Gavel, W.E. Hatfield, D.J. Hodgson, Inorg. Chem. 17 (1978) 1415.
[39] R.F. Drake, V.H. Crawford, W.E. Hatfield, J. Chem. Phys. 60 (1974) 4525.
[40] N.S. Gill, M. Sterns, Inorg. Chem. 9 (1970) 1619.
[41] J.A. Bertrand, J.A. Kelley, J. Am. Chem. Soc. 88 (1966) 4746.
[42] H. Bock, H. tom Dieck, H. Pyttlik, M. Schnöller, Z. Anorg. Allg. Chem. 357 (1968) 54.
[43] F.S. Keij, J.G. Haasnoot, A.J. Oosterling, J. Reedijk, C.J. O'Connor, J.H. Zhang, A.L. Spek, Inorg. Chim. Acta 181 (1991) 185.
[44] A.W. Addison, T.N. Rao, J. Reedijk, J. van Rijn, G.V. Verschoor, J. Chem. Soc., Dalton Trans. (1984) 1349.
[45] S.K. Hoffmann, D.K. Towle, W.E. Hatfield, K. Wieghardt, P. Chaudhuri, J. Weiss, Mol. Cryst. Liq. Cryst. 107 (1984) 161.
[46] K. Nakamoto, Infrared and Raman Spectra of Inorganic and Coordination Compounds, fourth ed., Wiley, New York, 1986.
[47] B. Bleaney, K.D. Bowers, Proc. R. Soc. London Ser. A 214 (1952) 451.
[48] J.W. Stout, R.C. Chisholm, J. Chem. Phys. 36 (1962) 979.
[49] T. Watanabe, J. Phys. Soc. Jpn. 17 (1962) 1856.
[50] J.N. McElearney, S. Merchant, R.L. Carlin, Inorg. Chem. 12 (1973) 906.
[51] O. Kahn, Molecular Magnetism, VCH Publishers, New York, 1993.
[52] C.J. O' Connor, Inorg. Chim. Acta 127 (1987) L29.
[53] D.H. Svedung, Acta Chem. Scand. 23 (1969) 2865.
[54] S.J. Brown, X. Tao, T.A. Wark, D.W. Stephan, P.K. Mascharak, Inorg. Chem. 27 (1988) 1581.
[55] E.D. Estes, W.E. Estes, W.E. Hatfield, D.J. Hodgson, Inorg. Chem. 14 (1975) 106.
[56] T. Rojo, M.I. Arriortua, J. Ruiz, J. Darriet, G. Villeneuve, D. Beltran-Porter, J. Chem. Soc., Dalton Trans. (1987) 285.
[57] A. Tosik, W. Maniukiewicz, M. Bukowska-Strzyzewska, J. Mrozinski, M.P. Sigalas, C.A. Tsipis, Inorg. Chim. Acta 190 (1991) 193.
[58] D.J. Hodgson, P.K. Hale, W.E. Hatfield, Inorg. Chem. 10 (1971) 1061.
[59] J.A. Carrabine, M. Sundaralingam, J. Am. Chem. Soc. 92 (1970) 369.
[60] K.T. McGregor, W.E. Hatfield, J. Chem. Phys. 65 (1976) 4155.